

# Learning Temporal Quantum Tomography

Quoc Hoan Tran<sup>\*</sup> and Kohei Nakajima<sup>†</sup>  
 Graduate School of Information Science and Technology,  
 The University of Tokyo, Tokyo 113-8656, Japan  
 (Dated: March 1, 2025)

Quantifying and verifying the control level in preparing a quantum state are central challenges in building quantum devices. The quantum state is characterized from experimental measurements, using a procedure known as tomography, which requires a vast number of resources. Furthermore, the tomography for a quantum device with temporal processing, which is fundamentally different from the standard tomography, has not been formulated. We develop a practical and approximate tomography method using a recurrent machine learning framework for this intriguing situation. The method is based on repeated quantum interactions between a system called quantum reservoir with a stream of quantum states. Measurement data from the reservoir are connected to a linear readout to train a recurrent relation between quantum channels applied to the input stream. We demonstrate our algorithms for quantum learning tasks followed by the proposal of a quantum short-term memory capacity to evaluate the temporal processing ability of near-term quantum devices.

*Introduction.*— The impressive progress in realizing quantum-enhanced technologies places a demand on the characterization and validation of quantum hardware. One of the most quintessential parts of building quantum devices is quantum process tomography (QPT), which is used in verifying quantum devices via the reconstruction of an unknown quantum channel from measurement data. In general, exact QPT is difficult due to the exponential scaling of the required measurement bases and classical postprocessing with the number of qubits in the system. Moreover, performing measurements on different bases leads to the reconfiguration of the experimental setup, which is challenging in real implementations. Consequently, exact QPT has only been explored in small system sizes up to three qubits [1–5], though this can be improved using an approximate characterization such as the tensor network representation of the quantum channel with a data-driven optimization [6].

Previous QPT approaches assume that the quantum device processes in a time-independent behavior. We consider a general scenario when quantum states come in a sequence, and the output of the quantum device is based on the previous input states. Given a sequence of input states  $\beta_1, \beta_2, \dots$  in a Hilbert space  $\mathcal{H}_A$  with the dimension  $D_A$ , a natural example is the reproducing of previous states, where the device stands for a temporal map  $\mathcal{F}(\beta_n) = \beta_{n-d}$  with  $d \geq 0$  is a delay parameter. Another example is the temporal depolarizing channel  $\mathcal{F}(\beta_n) = p_n \frac{I}{D_A} + (1 - p_n)\beta_n$ , which replaces  $\beta_n$  with a completely mixed state  $I/D_A$  with probability  $p_n$  and leaves the state untouched otherwise. Generally, given a sequence  $\Omega_1, \Omega_2, \dots$  of unknown quantum channels from  $\mathcal{H}_A$  to another Hilbert space, we consider  $\mathcal{F}$  as

$$\mathcal{F}(\beta_n) = \frac{1}{Z} \sum_{i=0}^d \eta_i \Omega_{n-i}(\beta_{n-i}), \quad (1)$$

where  $\eta_i$  are unknown non-negative real numbers with  $Z = \sum_{i=0}^d \eta_i$  to preserve the trace. Our objective is to

characterize  $\mathcal{F}$  from measurement data. It is much more complicated than the standard QPT since  $\mathcal{F}$  is not a quantum channel and each  $\Omega_{n-i}$  operates in time-delayed states. The tomography of  $\mathcal{F}$  can only be reconstructed via the action to each input sequence.

In this Letter, we propose a supervised learning framework to perform the approximate tomography of  $\mathcal{F}$ . We consider a quantum system  $\mathcal{S}$  as interacting with a stream of external quantum states,  $\beta_1, \beta_2, \dots$ , belonging to another system  $\mathcal{E}$ . Each  $\beta_n$  interacts for a certain time with  $\mathcal{S}$  before being replaced by another one. We refer to  $\mathcal{S}$  as the *main system* or a *quantum reservoir* (QR) to perform the temporal quantum processing task, and  $\mathcal{E}$  as an *auxiliary system* to store the states interacting with  $\mathcal{S}$ . The information of external states is sequentially transferred from  $\mathcal{E}$  into  $\mathcal{S}$  with a recurrent relation. The measurements of observables in  $\mathcal{S}$  can be used in a classical training machine to reconstruct the density matrix for the output of  $\mathcal{F}$  (Fig. 1). We establish the tomography of temporal maps with high fidelities in several quantum tasks. We further propose a concept of quantum short-term memory capacity to evaluate the ability of reconstructing temporal density matrices. Our study aims to uncover the temporal processing ability of near-term quantum devices and provides a perspective on utilizing classical machine learning methods in quantum tasks.

*Model.*— A single interaction between the main system and the auxiliary system is described below. Assume that the initial state of the coupled system  $(\mathcal{S}, \mathcal{E})$  is a product state  $\varrho = \rho \otimes \beta$ , where  $\rho$  and  $\beta$  are the state of  $\mathcal{S}$  and the reference state of  $\mathcal{E}$ , respectively. The coupled system is evolved under a unitary evolution  $U$  with the reduced state in  $\mathcal{S}$  as  $\rho' = \mathcal{L}_\beta(\rho) = \text{Tr}_\mathcal{E}[U(\rho \otimes \beta)U^\dagger]$ . Here,  $\mathcal{L}_\beta$  is called the *reduced dynamics map*, which is a completely positive and trace-preserving (CPTP) map. The successive interactions are described via the recurrent relation

$$\rho_n = \mathcal{L}_{\beta_n}(\rho_{n-1}) = \text{Tr}_\mathcal{E}[U(\rho_{n-1} \otimes \beta_n)U^\dagger], \quad (2)$$

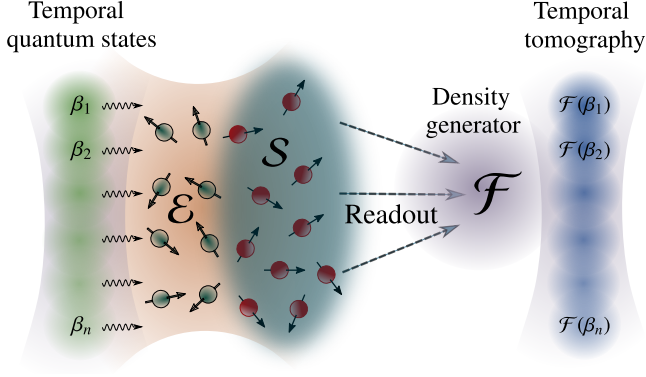


FIG. 1. The target of learning temporal tomography is to reconstruct the density of a temporal quantum map  $\mathcal{F}$  applied to a sequence of input states. The output of this map is based on the previous input states. Our system consists of a *quantum reservoir*  $\mathcal{S}$  interacting with a stream of input states in an auxiliary system  $\mathcal{E}$ . The inputs are then processed by some cycles of the time evolution, each cycle is followed by the measurement of  $\mathcal{S}$ . These measurement results are used in a readout layer to emulate the behavior of  $\mathcal{F}$ .

where  $\rho_n$  is the state of  $\mathcal{S}$  for the  $n$ th interaction.

We obtain partial information by measuring local observables  $O_1, O_2, \dots, O_K$  on the state  $\rho_n$ . The theory of quantum steering says that there will be a way to perform these measurements without disturbing the state of  $\mathcal{E}$  on average. We obtain a state called *reservoir state*  $\mathbf{x}_n$ , where its  $k$ th element  $x_{nk}$  can be calculated as  $x_{nk} = \text{Tr}[O_k \rho_n] = \langle O_k \rangle_{\rho_n}$ , which is the expectation of the measurement result via  $O_k$  on  $\rho_n$ . One can increase the dimension of  $\mathbf{x}_n$  by performing measurements at multiple times. Between two inputs,  $M$  cycles of the unitary evolution are processed and each of them is followed by a measurement.  $M$  is called the measurement multiplexity, thus we obtain  $MK$  elements in each reservoir state. In experimental realizations, the effect of measurement back-action should be avoided. One promising solution is considering multiple copies of same systems such as a huge ensemble of identical molecules in the nuclear magnetic resonance system [7–9]. This measurement back-action problem can be less serious for the temporal processing when the information of quantum channels is encoded in a long-enough stream of learning data.

In learning the tomography of  $\mathcal{F}$ , we are given an input sequence of states  $\{\beta_1, \dots, \beta_L\}$  and the corresponding target sequence  $\hat{\mathbf{y}} = \{\hat{\mathbf{y}}_1, \dots, \hat{\mathbf{y}}_L\}$  where  $\hat{\mathbf{y}}_k \in \mathbb{R}^d$  is the real vector form to stack the real and imaginary elements of  $\mathcal{F}(\beta_k)$ . Let  $\mathcal{X} \subset \mathbb{R}^K$  denote the space of reservoir states  $\mathbf{x}_n$ . Our framework includes a readout map  $h: \mathcal{X} \rightarrow \mathbb{R}^d$ , which is simply taken as a linear combination of the reservoir states as  $\mathbf{y}_n = h(\mathbf{x}_n) = \mathbf{w}^\top \mathbf{x}_n$ . Here,  $\mathbf{w}$  is the parameter to be optimized by minimizing the mean-square error between  $\mathbf{y}_n$  and  $\hat{\mathbf{y}}_n$  over  $n = 1, \dots, L$  (see [10]). Since the target of tomography is the density

matrix of a physical state, we use the fidelity to estimate the predict error. Given two density matrices  $\rho$  and  $\sigma$ , the fidelity  $F$  is generally defined as the quantity  $F(\rho, \sigma) = \left( \text{Tr}[\sqrt{\sqrt{\sigma}\rho\sqrt{\sigma}}] \right)^2$ . In error-free tomography,  $F = 1$ , and  $F < 1$  otherwise. In the evaluation stage, we are given an input sequence  $\{\beta_{L+1}, \dots, \beta_{L+T}\}$  with the corresponding target  $\{\hat{\sigma}_{L+1}, \dots, \hat{\sigma}_{L+T}\}$  where  $\hat{\sigma}_i = \mathcal{F}(\beta_i)$ . The reconstructed output sequence is  $\{\mathbf{y}_{L+1}, \dots, \mathbf{y}_{L+M}\}$ , which is rearranged in the matrix form  $\{\sigma_{L+1}, \dots, \sigma_{L+T}\}$  [11]. To evaluate the training performance, we calculate the root mean square of the

evaluation stage as  $\text{RMSF} = \sqrt{\frac{1}{T} \sum_{i=L+1}^{L+T} F^2(\hat{\sigma}_i, \sigma_i)}$ .

*Transient dynamics characterization.*— Since the reservoir states are obtained from the quantum evolution, the learning and prediction should be performed in a reproducible way. That is, the QR should produce the trajectories that are independent of its initial state for the same input sequence. We refer this as quantum echo state property (QESP) [12, 13]. In the following, we consider the Schatten 1-norm, defined by  $\|A\| = \text{Tr}[\sqrt{A^\dagger A}]$  for matrix  $A$ . We denote  $\Phi_n = \mathcal{L}_{\beta_n} \mathcal{L}_{\beta_{n-1}} \dots \mathcal{L}_1$ , then  $\Phi_n$  is a CPTP map and  $\rho_n = \Phi_n(\rho_0)$ . Given  $\varepsilon > 0$ , a QR is said to satisfy the  $\varepsilon$ -QESP if for any input sequence there exists a smallest integer number  $T(\varepsilon)$  such that  $\|\Phi_n(\rho_0^{(1)}) - \Phi_n(\rho_0^{(2)})\| < \varepsilon$  for all  $n \geq T(\varepsilon)$  and all initial states  $\rho_0^{(1)}, \rho_0^{(2)}$ . The maximum  $T(\varepsilon)$  for all input sequences is defined as the  $\varepsilon$ -QESP time scale.

We demonstrate that the  $\varepsilon$ -QESP time scale can be evaluated via the spectrum of  $\mathcal{L}_n$ . First, we consider the constant input  $\beta_n = \beta$ , then  $\mathcal{L}_{\beta_n} = \mathcal{L}$  for all  $n$ . The spectrum of  $\mathcal{L}$  can be written as  $1 = |\lambda_1| \geq |\lambda_2| \geq \dots \geq |\lambda_s|$ , where  $\lambda_j$  is the  $j$ th eigenvalue of  $\mathcal{L}$ . Because  $\mathcal{L}$  can be a non-Hermitian map, it can have both left ( $L_j$ ) and right ( $R_j$ ) eigenmatrices corresponding to  $\lambda_j$ . We choose the normalization  $\text{Tr}(L_k R_l) = \delta_{kl}$  and  $\text{Tr}[R_1] = 1$ . Any density matrix  $\rho$  can be written as a vectorized form  $\text{vec}(\rho)$  using the Choi-Jamiolkowski isomorphism, which is the same as stacking columns of  $\rho$ . Then,  $\mathcal{L}$  can be expressed as a matrix  $\tilde{\mathcal{L}}$ , such that  $\text{vec}(\rho_n) = \tilde{\mathcal{L}} \text{vec}(\rho_{n-1}) = \tilde{\mathcal{L}}^n(\text{vec}(\rho_0))$ . Therefore, we have

$$\text{vec}(\rho_n) = \text{vec}(R_1) + \sum_{j=2}^s b_j \lambda_j^n \text{vec}(R_j), \quad (3)$$

where  $b_j = \text{Tr}[L_j \rho_0]$ . If  $|\lambda_2|^{-1} > 1$ , the steady state  $\rho_{ss}$  of the system is unique ( $\rho_{ss} = R_1$ ) with the convergence rate depending on the magnitude of  $|\lambda_2|^{-1}$ , i.e.,  $\|\rho_n - \rho_{ss}\| \sim e^{-n/N}$  with  $N \sim \frac{1}{\ln(|\lambda_2|^{-1})}$ . The QESP is satisfied that we can evaluate the  $\varepsilon$ -QESP time scale as  $O(\frac{\ln(\varepsilon^{-1})}{\ln(|\lambda_2|^{-1})})$ .

To further understand the transient dynamics, we observe that each  $\lambda_j$  such that  $|\lambda_j| < 1$  represents a time scale of the system. Let us assume that  $|\lambda_2| < 1$  and there is a large separation between  $|\lambda_m|$  and  $|\lambda_{m+1}|$

in the spectrum of  $\mathcal{L}$  as  $|\lambda_m| \gg |\lambda_{m+1}|$ . This separation corresponds to two scales:  $N_1 = \frac{1}{\ln(|\lambda_{m+1}|^{-1})}$  and  $N_2 = \frac{1}{\ln(|\lambda_m|^{-1})}$ . If  $n \gg N_2$ , we can ignore the terms with  $\lambda_j^n$  in Eq. (3) for all  $|\lambda_j| < 1$ . If  $n \gg N_1$ , only  $\lambda_j^n$  with  $j \leq m$  contribute to the dynamics of the system. If  $N_1 \ll n \ll N_2$ , the metastability occurs and the system relaxes into a state in metastable manifold (MM) [14]. Here, MM is a convex subset of the system states on which the long-time dynamics are described via the motion towards the true stationary state, which is reached at  $n \gg N_2$ .

Next, we consider the input as a sequence of independent and identically distributed (i.i.d.) random states. We obtain a sufficient check for the  $\varepsilon$ -QESP time scale via the contraction coefficient of  $\mathcal{L}_\beta$ . Here, a CPTP map  $\mathcal{L}$  has the contraction coefficient  $c(\mathcal{L})$  ( $0 < c(\mathcal{L}) \leq 1$ ) if  $c(\mathcal{L})$  is the smallest number such that for any pair of density operators  $\rho, \sigma$  in its domain,  $\|\mathcal{L}(\rho) - \mathcal{L}(\sigma)\| \leq c(\mathcal{L})\|\rho - \sigma\|$ . If there exist  $n_0$  such that  $\mu = \max(c(\mathcal{L}_{\beta_n})) < 1$  for all  $n \geq n_0$ , then the  $\varepsilon$ -QESP time scale can be evaluated as  $O(\frac{\ln(\varepsilon^{-1})}{\ln(\mu^{-1})})$  (see proof in [10]).

To numerically investigate the transient dynamics, we consider a specific system modeled by the transverse field Ising model, where the Hamiltonian is given by

$$H = - \sum_{i>j=1}^N J_{i,j} \hat{s}_i^x \hat{s}_j^x - B \sum_j^N \hat{s}_j^z. \quad (4)$$

Here,  $B$  is the natural frequency of 1/2-spins represented for qubits and  $\hat{s}_j^\gamma$  ( $\gamma \in \{x, y, z\}$ ) are the Pauli operators measuring the qubit  $j$  along the  $\gamma$  direction. The coupling coefficients  $J_{ij}$  between spins can be randomly selected or be fixed depending on the distance of interaction [15]. To describe our QR, we assume that the auxiliary system  $\mathcal{E}$  includes the first  $N_e$  spins where the remaining  $N_m = N - N_e$  spins form the reservoir  $\mathcal{S}$ . We present the setting of *power-law decaying* for  $J_{ij} = J|i - j|^{-\alpha}/N(\alpha)$  with an interaction strength  $J$ , power coefficient  $\alpha$  ( $0 < \alpha < 3$ ), and normalization constant  $N(\alpha) = \frac{1}{N-1} \sum_{i>j} |i - j|^{-\alpha}$ . The coupled system  $(\mathcal{S}, \mathcal{E})$  is a closed system with the total Hamiltonian  $H$  unchanged during each interaction. We consider the model parameters  $\alpha = 1, J = 1, J/B = 1$ , and the unitary  $U = \exp(-i\tau H)$ , where  $\tau$  is the interaction time.

The dynamics of QR is studied via the eigenvalues distribution of the reduced dynamics map  $\mathcal{L}_\beta$ . We first measure the ratios in absolute values between two consecutive eigenvalues as  $r_k = |\lambda_{k+1}|/|\lambda_k|$ , which indicate the separation of time scales in the dynamics. In Fig. 2, the top panel shows the expectation value of  $r_k$  over  $k$  according to the normalized time  $\tau B$  for 100 random  $\mathcal{L}_\beta$  with  $N_m = 4, N_e = 2$ . The bottom panel displays exemplary distributions of eigenvalues for  $\tau B = 0.5, 1.5, 2.5, 5.0, 10.0$ . If

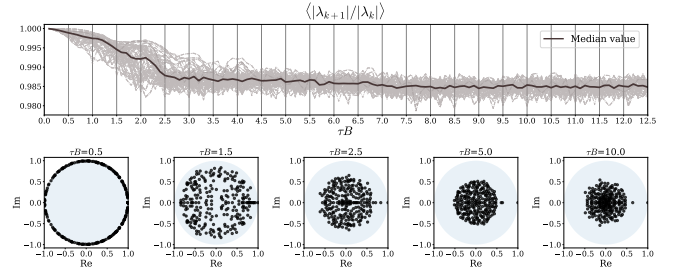


FIG. 2. (Top) The values of  $\langle |\lambda_{k+1}|/|\lambda_k| \rangle$  for 100 random reduced dynamics maps  $\mathcal{L}_\beta$  with  $N_m = 4, N_e = 2, \alpha = 1, J = 1$ , and  $J/B = 1$ . The solid line depicts the median value of the ensemble of dynamics maps. (Bottom) The distribution of eigenvalues in the unit disk at  $\tau B = 0.5, 1.5, 2.5, 5.0, 10.0$ .

the eigenvalues are close to the unit border or  $r_k$  are close to 1,  $\mathcal{L}_\beta$  reduces toward a unitary map and the QR relaxes into a state on a high-dimensional MM. Such long-time dynamics makes the QR retain the information of its initial states on this MM. We observe the transition ( $1.5 \leq \tau B \leq 2.5$ ) from high values to a stable range of  $\langle r_k \rangle$ . In the stable range, more eigenvalues are moved toward the center of the unit disk, the contraction coefficients  $c(\mathcal{L}_\beta)$  become smaller. The effects of initial states are reduced, and the dynamics will be characterized by lower-dimensional MMs in a more ergodic phase with a favorable convergence property (see [10]).

*Temporal tomography.*—We present concrete applications of the temporal tomography with the model in Eq. (4). We consider a sequence of i.i.d. random density matrices  $\beta_1, \beta_2, \dots$  and temporal map  $\mathcal{F}$  in Eq. (1), where each channel  $\Omega_n$  acts on  $D \times D$  density matrices to return  $D \times D$  density matrices, where  $D = 2^{N_e}$ . We select  $K = N_m$  observables  $O_j = \hat{s}_j^z$  as the projections of spins over the  $z$ -axis to produce the readout reservoir states. In principle, we can consider other observables such as the spins correlations  $\hat{s}_i^z \hat{s}_j^z$ . In fact, if the channel  $\Omega_n$  is time-independent, it can be described by  $D^4 - D^2$  independent parameters. Therefore the reservoir states can characterize the time-independent channel if  $KM \geq D^4 - D^2$  [16]. Our situation is more tricky with time-dependent channels. If  $\eta_i = 1$  for all  $i$ , we can consider  $\mathcal{F}$  as a quantum version of the simple moving average filter for a sequence of quantum channels acting on the input states. If  $\eta_i = (d + 1 - i)$  for all  $i$ , we have a weighted moving average filter. If  $\eta_d = 1$  and  $\eta_i = 0$  for  $i \neq d$ , we have a reconstruction of the channels on  $d$ -delay input states.

We first consider the delay-reconstruction task, where  $\{\beta_n\}$  is an i.i.d. sequence and  $\mathcal{F}(\beta_n) = \beta_{n-d}$ . This task allows us to investigate the *short-term memory* (STM) of the system, where the output states should depend significantly on the recent input states. In classical information processing, the STM is defined via the coefficient of determination to measure how much variance of the

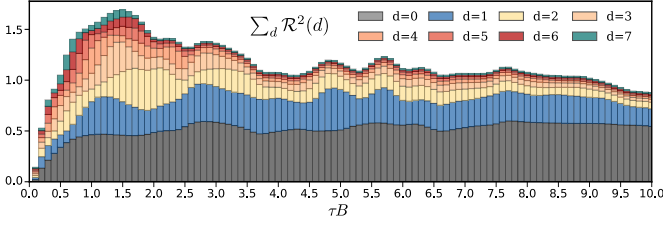


FIG. 3. The total quantum short-term memory  $\sum_d \mathcal{R}^2(d)$  broken down in different  $d$  ( $0 \leq d \leq 7$ ) according to  $\tau B$  with  $\alpha = 1.0, J = 1.0, J/B = 1.0, N_e = 2$ , and  $N_m = 4$ .

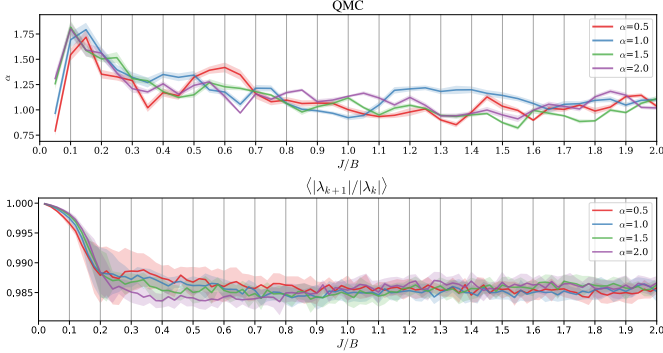


FIG. 4. (Top) Quantum short-term memory capacity as the function of model parameters  $\alpha$  and  $J/B$  with  $N_e = 2, N_m = 4$ , and  $\tau B = 10.0$ . (Bottom) The statistic value  $\langle |\lambda_{k+1}|/|\lambda_k| \rangle$  over  $k$  as the function of model parameters. The shaded areas indicate the confidence intervals (one standard deviation) calculated in the same ensemble of runs.

delay inputs can be recovered from outputs [17]. Since the input and output of our framework are density matrices, we define the  $d$ -delay quantum STM capacity of the QR by the square of the distance correlation [18]  $\mathcal{R}^2(d)$  between the output  $\{\sigma_n\}$  and the target  $\{\hat{\sigma}_n\} = \{\beta_{n-d}\}$ :

$$\mathcal{R}^2(d) = \frac{\mathcal{V}^2(\{\sigma_n\}, \{\hat{\sigma}_n\})}{\sqrt{\mathcal{V}^2(\{\sigma_n\})\mathcal{V}^2(\{\hat{\sigma}_n\})}}. \quad (5)$$

Here,  $\mathcal{V}^2(\{\sigma_n\}, \{\hat{\sigma}_n\})$  and  $\mathcal{V}^2(\{\sigma_n\}) = \mathcal{V}^2(\{\sigma_n\}, \{\sigma_n\})$  represent for the distance covariance and distance standard deviation (see [10]).  $\mathcal{R}^2(d)$  is between 0 and 1, and represents the fraction of distance variance explainable in the sequence of output states by the sequence of delayed input states. We then define the quantum STM capacity,  $\text{QMC} = \sum_{d=0}^{\infty} \mathcal{R}^2(d)$ , to measure how much distance variance of the delay input states can be recovered from output states, summed over all delays. The QMC is generally proposed as a standard quantity to compare the temporal processing capacity of quantum devices.

Figure 3 shows the total memory  $\sum_d \mathcal{R}^2(d)$  as a function of  $\tau B$  broken down in values of  $d$  with the model parameters  $\alpha = 1.0, J = 1.0, J/B = 1.0$ , and  $N_e = 2, N_m = 4$ . The first 1000 time steps are excluded for initial transients to satisfy the QESP. The training and evaluating are performed with 3000 and 1000 time steps, respec-

tively. The value of  $\mathcal{R}^2(d)$  is averaged over different runs with ten random trials of the initial state and input sequence. This value is faded out as increasing the delay  $d \geq 7$ . The total  $\sum_{d=0}^{d=7} \mathcal{R}^2(d)$  increases and obtains the peak value at the onset of the transition region from more unitary ( $\tau B \leq 1.5$ ) to more ergodic behavior ( $\tau B \geq 2.5$ ) in Fig. 2. We further examine the relation between the QMC and other Ising model parameters such as  $\alpha$  and  $J/B$ . The top panel of Fig. 4 displays the average QMC of 10 random trials as the function of  $\alpha$  and  $J/B$  for  $N_e = 2, N_m = 4$ , and  $\tau B = 10.0$ . The values of  $\mathcal{R}^2(d)$  is calculated until  $d_{\max} = 10$ . We also plot the statistic value  $\langle |\lambda_{k+1}|/|\lambda_k| \rangle$  averaged over 100 random  $\mathcal{L}_\beta$  to see the dynamical transition of the eigenvalues' distribution from more unitary ( $J/B < 0.1$ ) to more ergodic behavior ( $J/B > 0.2$ ). Interestingly, QMC achieves highest values in this transition region as  $0.1 < J/B < 0.2$  (see [10] for results with other  $\tau B$ ). These intriguing results remind us of the well-known phenomenon in classical reservoir processing, where in some situations, a short-term memory capacity achieves the maximum values at the edge of stability between different dynamic regimes [19]. For nonlinear and temporal classical tasks in spin networks, the similar observations have also been investigated recently to address the impact of the transition between localization and thermalization manifest [20].

Finally, we demonstrate the reconstruction of depolarizing quantum channel  $\mathcal{F}(\beta_n) = \Omega_{n-d}(\beta_{n-d})$  (see [10] for the demonstration of other tasks). Here, we set  $\Omega_n$  as the time-dependent depolarizing quantum channel  $\Omega_n(\beta) = p_n \frac{I}{D} + (1 - p_n)\beta$ . The depolarizing probability  $p_n$  is formulated as the  $r$ th-order nonlinear dynamical output:  $p_n = \kappa p_{n-1} + \eta p_{n-1} \left( \sum_{j=0}^{r-1} p_{n-j-1} \right) + \gamma u_{n-r+1} u_n + \delta$ , where  $r = 10, \kappa = 0.3, \eta = 0.04, \gamma = 1.5$ , and  $\delta = 0.1$ . Here,  $\{u_n\}$  is a random sequence of scalar values in  $[0, 0.2]$  to set  $p_n$  into the stable range in  $[0, 1]$  [21]. This setting introduces the temporal dependency between quantum channels. We consider  $d = 1$  as an interesting situation, where our scheme must memorize both the previous input states and previous quantum channel applied to this state. The number of time steps used in the initial transients, training, and evaluation phases are 1000, 3000, and 1000, respectively. Figure 5 illustrates the calculated error (1.0 - RMSF) as functions of  $\tau B$  with the measurement multiplexity  $M = 5$  for different values of  $N_e, N_m$  and  $K$ . The number of observables is set to  $K = N_m$  if we only select the observables as spin projections  $O_j = \hat{s}_j^z$  for all  $j$ , and to  $K = N_m(N_m + 1)/2$  if we further select the observables as two-spins correlations  $\hat{s}_i^z \hat{s}_j^z$  for all  $i < j$ . The error is averaged over ten different runs with random trials of the input sequence and initial state. We confirm that increasing  $N_m, M$  and  $K$  indeed scales the fidelity [22] (see full results in [10]). The fidelity is larger than 96% for the QR of  $N_m = 5$  qubits and input states of  $N_e = 2$  qubits with almost values of  $\tau B$ . The fidelity is



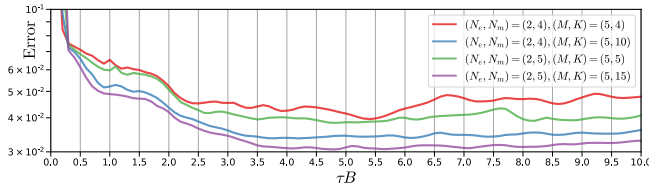


FIG. 5. Tomography errors ( $1.0 - \text{RMSF}$ ) as functions of  $\tau B$  for the reconstruction of depolarizing quantum channel  $\mathcal{F}(\beta_n) = \Omega_{n-d}(\beta_{n-d})$  with  $d = 1$ .

larger than 94% even with  $N_e = 3$  qubits and  $N_m = 4, 5$  (see [10]). Particularly, for  $N_m = 4, 5$  and  $N_e = 2$ , the error reduces quickly to the lower values in the region of  $1.5 < \tau B < 2.5$  in Fig. 5. To refer to the statistics levels of eigenvalues in Fig. 2 for  $N_m = 4$ , this region is similar to the range of  $\tau B$  for the transition of  $r_k$  to the relaxation in the low-dimensional MM. This observation with the results in the QMC indicate that the statistics levels of eigenvalues of reduced dynamic maps are helpful in the setting of parameters for enhancing the performance of tomography tasks in future experimental implementations [8, 23, 24].

*Conclusion.*— We formulate and propose the general framework of tomography for quantum maps acting on temporal quantum data. We establish the general conditions via the dynamics maps to enhance the convergence property and the processing ability in quantum tasks, such as the quantum short-term memory capacity. A potential future direction is to develop the theoretical magnitude on the temporal memory property of near-term quantum devices.

\* [tran.qh@ai.u-tokyo.ac.jp](mailto:tran.qh@ai.u-tokyo.ac.jp)

† [k.nakajima@mech.t.u-tokyo.ac.jp](mailto:k.nakajima@mech.t.u-tokyo.ac.jp)

- [1] J. L. O’Brien, G. J. Pryde, A. Gilchrist, D. F. V. James, N. K. Langford, T. C. Ralph, and A. G. White, *Phys. Rev. Lett.* **93**, 080502 (2004).
- [2] M. Riebe, K. Kim, P. Schindler, T. Monz, P. O. Schmidt, T. K. Körber, W. Hänsel, H. Häffner, C. F. Roos, and R. Blatt, *Phys. Rev. Lett.* **97**, 220407 (2006).
- [3] R. C. Bialczak, M. Ansmann, M. Hofheinz, E. Lucero, M. Neeley, A. D. O’Connell, D. Sank, H. Wang, J. Wenner, M. Steffen, A. N. Cleland, and J. M. Martinis, *Nature Physics* **6**, 409 (2010).
- [4] A. Shabani, R. L. Kosut, M. Mohseni, H. Rabitz, M. A. Broome, M. P. Almeida, A. Fedrizzi, and A. G. White, *Phys. Rev. Lett.* **106**, 100401 (2011).
- [5] L. C. G. Govia, G. J. Ribell, D. Ristè, M. Ware, and H. Krovi, *Nature Communications* **11** (2020), 10.1038/s41467-020-14873-1.
- [6] G. Torlai, C. J. Wood, A. Acharya, G. Carleo, J. Carrasquilla, and L. Aolita, *Preprint at arXiv:2006.02424* (2020).
- [7] K. Fujii and K. Nakajima, *Phys. Rev. Applied* **8**, 024030 (2017).

- [8] M. Negoro, K. Mitarai, K. Fujii, K. Nakajima, and M. Kitagawa, *Preprint at arXiv:1806.10910* (2018).
- [9] K. Nakajima, K. Fujii, M. Negoro, K. Mitarai, and M. Kitagawa, *Phys. Rev. Applied* **11**, 034021 (2019).
- [10] See Supplemental Materials.
- [11] For sufficient training samples, the simple training process in our framework can reconstruct the density matrices, which are positive semidefinite. However, due to statistical fluctuations, there are some cases in which the reconstructed matrix  $A$  is not positive semidefinite. We project  $A$  onto the spectrahedron to obtain a positive semidefinite matrix  $\hat{A}$  such that the trace of  $\hat{A}$  is equal to 1 and the Frobenius norm between  $A$  and  $\hat{A}$  is minimized [25].
- [12] J. Chen and H. I. Nurdin, *Quantum Inf. Process.* **18** (2019), 10.1007/s11128-019-2311-9.
- [13] Q. H. Tran and K. Nakajima, *Preprint at arXiv:2006.08999* (2020).
- [14] Metastability is a characteristic feature of the dynamics of a slow relaxing system with the partial relaxation into long-lived states before eventual decay to the true stationary state. Metastability appears due to the separation of time scales in the dynamics; therefore, different initial states of the QR will relax to different metastable states in the transient dynamics.
- [15] Regarding the practical feasibility, we note that there are two physical implementations of the transverse field Ising model, such as in the NMR spin ensemble in a molecular solid [7, 8] or in a trapped-ion quantum simulation [26–28].
- [16] S. Ghosh, A. Opala, M. Matuszewski, T. Paterek, and T. C. H. Liew, *IEEE Trans. Neural Netw. Learn. Syst.*, **1** (2020).
- [17] H. Jaeger, “Short term memory in echo state networks,” (GMD-Forschungszentrum Informationstechnik, 2001).
- [18] G. J. Székely, M. L. Rizzo, and N. K. Bakirov, *Ann. Stat.* **35**, 2769 (2007).
- [19] P. Barančok and I. Farkaš, in *Artificial Neural Networks and Machine Learning – ICANN 2014* (Springer International Publishing, 2014) pp. 41–48.
- [20] R. Martínez-Peña, G. L. Giorgi, J. Nokkala, M. C. Soriano, and R. Zambrini, *Preprint at arXiv:2103.05348* (2021).
- [21] The sequence  $\{p_n\}$  resembles the NARMA benchmark [29], which is commonly used for evaluating the computational capability of temporal processing with long time dependence.
- [22] Related to the quantum Zeno effect [30], we should not set the value  $\tau B/M$  as too small, since in this case, the time evolution slows down and the frequent measurements force the quantum state to remain in a projected subspace.
- [23] J. Chen, H. I. Nurdin, and N. Yamamoto, *Phys. Rev. Applied* **14**, 024065 (2020).
- [24] P. Mujal, R. Martínez-Peña, J. Nokkala, J. García-Bení, G. L. Giorgi, M. C. Soriano, and R. Zambrini, *Preprint at arXiv:2102.11831* (2021).
- [25] Y. Chen and X. Ye, *Preprint at arXiv:1101.6081* (2011).
- [26] D. Porras and J. I. Cirac, *Phys. Rev. Lett.* **92**, 207901 (2004).
- [27] K. Kim, M.-S. Chang, R. Islam, S. Korenblit, L.-M. Duan, and C. Monroe, *Phys. Rev. Lett.* **103**, 120502 (2009).
- [28] P. Jurcevic, B. P. Lanyon, P. Hauke, C. Hempel, P. Zoller,

- R. Blatt, and C. F. Roos, [Nature](#) **511**, 202 (2014).
- [29] A. Atiya and A. Parlos, [IEEE Trans. Neural Netw. Learn. Syst.](#) **11**, 697 (2000).
- [30] B. Misra and E. C. G. Sudarshan, [J. Math. Phys.](#) **18**, 756 (1977).

# Supplementary Material for “Learning Temporal Quantum Tomography”

Quoc Hoan Tran<sup>\*</sup> and Kohei Nakajima<sup>†</sup>  
*Graduate School of Information Science and Technology,  
The University of Tokyo, Tokyo 113-8656, Japan*  
(Dated: March 1, 2025)

This supplementary material describes in detail the calculations, the experiments introduced in the main text, and the additional figures. The equation, figure, and table numbers in this section are prefixed with S (e.g., Eq. (S1) or Fig. S1, Table S1), while numbers without the prefix (e.g., Eq. (1) or Fig. 1, Table 1) refer to items in the main text.

## CONTENTS

I. Learning the temporal tomography	2
A. Reservoir computing	2
B. Quantum reservoir computing	3
C. Learning the temporal tomography	3
II. Convergence analysis	4
III. Metastability analysis	7
IV. Quantum short-term memory capacity	10
V. Results on the temporal tomography tasks	13
References	17

---

<sup>\*</sup> [tran\\_qh@ai.u-tokyo.ac.jp](mailto:tran_qh@ai.u-tokyo.ac.jp)

<sup>†</sup> [k\\_nakajima@mech.t.u-tokyo.ac.jp](mailto:k_nakajima@mech.t.u-tokyo.ac.jp)

## I. LEARNING THE TEMPORAL TOMOGRAPHY

The proposed framework for learning the temporal tomography is a quantum extension of the classical reservoir computing (RC) to deal with quantum tasks. In this section, we first explain the principle of RC and then introduce some quantum extensions of RC in a scheme called quantum reservoir computing (QRC).

### A. Reservoir computing

Within machine learning (ML), the reservoir computing (RC) paradigm is a particular form of classical recurrent neural networks with random connectivity that can generate high-dimensional chaotic trajectories [1–3]. The crucial principle of RC is based on the modeling for the representation of the input sequence by feeding the input into a dynamical system called *the reservoir* to encode all relevant nonlinear dynamics. The reservoir is connected to the output by the *readout* part; only connections in this part are trained without affecting the reservoir dynamics. The RC paradigm is based on the following assumption: no knowledge of the system model, a large collection of measurement of readout, and the possibility to predict the target from the states encoded by the reservoir. Furthermore, the training mechanism is straightforward and computationally efficient, allowing RC to become particularly suitable for hardware implementations in various physical systems [4, 5].

We briefly explain here the standard pipeline of RC. In a general picture, the information processing in RC is described by the input-driven map  $G : \mathcal{S} \times \mathcal{X} \rightarrow \mathcal{X} \subset \mathbb{R}^K$ , where  $\mathcal{S}$  and  $\mathcal{X}$  are the input and the reservoir's state space, respectively. If we consider an infinite discrete-time input sequence  $\{\dots, \mathbf{s}_{-1}, \mathbf{s}_0, \mathbf{s}_1, \dots\}$  fed into the reservoir, the reservoir state  $\mathbf{x}_n$  is represented by the following recurrent relation:

$$\mathbf{x}_n = G(\mathbf{s}_n, \mathbf{x}_{n-1}). \quad (\text{S1})$$

In this way, the sequence  $\{\dots, \mathbf{x}_{-1}, \mathbf{x}_0, \mathbf{x}_1, \dots\}$  is the nonlinear transformation of the input sequence via the input-driven map implemented by a dynamical system. Therefore, the training in ML tasks can be separated to the reservoir so that we can reduce the computational cost by selecting a simple training procedure.

The RC paradigm can be used for both temporal and non-temporal supervised learning tasks. In temporal supervised learning tasks, we are given an input sequence  $\{\mathbf{s}_1, \dots, \mathbf{s}_L\}$  and the corresponding target sequence  $\hat{\mathbf{y}} = \{\hat{\mathbf{y}}_1, \dots, \hat{\mathbf{y}}_L\}$  where  $\hat{\mathbf{y}}_k \in \mathbb{R}^d$  with  $d$  is the output dimension. A RC system with temporal information processing ability includes a readout map  $h : \mathcal{X} \rightarrow \mathbb{R}^d$ , where the output signal  $\mathbf{y}_n$  is simply obtained from the readout map  $\mathbf{y}_n = h(\mathbf{x}_n)$  such that  $\mathbf{y}_n \approx \hat{\mathbf{y}}_n$  ( $n = 1, \dots, L$ ). The readout map is simply taken as a linear combination of the reservoir states as  $\mathbf{y}_n = h(\mathbf{x}_n) = \mathbf{w}^\top \mathbf{x}_n$ , where  $\mathbf{w}$  is the parameter and needs to be optimized. The training to adjust  $\mathbf{w}$  is performed by minimizing the error such as the mean-square error between  $\mathbf{y}_n$  and  $\hat{\mathbf{y}}_n$  over  $n = 1, \dots, L$ :

$$\text{MSE} = \frac{1}{L} \sum_{n=1}^L \|\mathbf{y}_n - \hat{\mathbf{y}}_n\|_2, \quad (\text{S2})$$

where  $\|\cdot\|_2$  denotes the Euclidean norm between two vectors in  $\mathbb{R}^d$ . For optimal training, a constant bias term  $x_{n,K+1} = 1$  is added to the reservoir state  $\mathbf{x}_n$ . A conventional approach is to optimize  $\mathbf{w}$  via the linear regression  $\hat{\mathbf{Y}} = \mathbf{X}\mathbf{w}$ , where  $\hat{\mathbf{Y}} = [\hat{\mathbf{y}}_1 \dots \hat{\mathbf{y}}_L]^\top$  is the  $L \times d$  target matrix and  $\mathbf{X}$  is the  $L \times (K+1)$  matrix that combines reservoir states  $\mathbf{x}_1, \mathbf{x}_2, \dots, \mathbf{x}_L$  of training data. The optimal value of  $\mathbf{w}$  is obtained via the Ridge regression in the matrix form  $\hat{\mathbf{w}}^\top = (\mathbf{X}^\top \mathbf{X} + \eta \mathbf{I})^{-1} \mathbf{X}^\top \hat{\mathbf{Y}}$ . Here,  $\eta$  is a positive constant shifting the diagonals introduced to avoid the problem of the near-singular moment matrix. The trained parameter  $\hat{\mathbf{w}}$  is used to generate outputs in the situation where we do not know about the target sequence and can only access the input sequence.

The information processing via the input-driven map is similar in non-temporal learning tasks, but the target is not the sequence but a specific value such as a label or a output vector corresponding with given input data. The input data are firstly converted into a sequence to be fed into the reservoir, then the reservoir states obtained from the reservoir dynamics are considered nonlinear features to learn the mapping to the output. The learning task is called regression or classification with respect to the property of output set as dense or discrete, respectively. In this way, the loss function measuring the prediction error can be designed in a flexible way in which we can apply more complicated training algorithms such as support vector machine or heuristic search methods to nonlinear optimization problems.



## B. Quantum reservoir computing

Quantum reservoir computing (QRC) is one of proposals to exploit the physical dynamics as a reservoir. Here, a disordered ensemble quantum dynamics system is used as a computational resource with the possibility of processing with an exponentially large number of degrees of freedom. The crucial idea is using a quantum system for obtaining the input-driven map defined in Eq. (S1). This input-driven map depends on the dynamical evolution of the quantum system and the quantum measurements to extract reservoir states from the system. For example, the reservoir can be implemented by a set of interacting qubits in the NMR system [6, 7], a set of fermions [8–10], a set of interacting quantum harmonic oscillators [11], or even a single nonlinear oscillator driven by a Hamiltonian dynamics [12]. The proof-of-principle experimental demonstrations for QRC are ongoing in the research with promising proposals for the NMR platform [13] and NISQ quantum computers [14, 15].

In our study, we model the QRC approach via the framework of repeated quantum interactions, which can be considered a general approach using the NMR system in Ref. [6]. In the repeated quantum interactions, input sequence is fed via the sequence interactions between reservoir system (called a *reduced quantum reservoir*)  $\mathcal{S}$  with a auxiliary system  $\mathcal{E}$ . The dynamical evolution is modeled by the following recurrent relation (Eq. 2 in our main text)

$$\rho_n = \mathcal{L}_{\beta_n}(\rho_{n-1}) = \text{Tr}_{\mathcal{E}}[U(\rho_{n-1} \otimes \beta_n)U^\dagger], \quad (\text{S3})$$

where  $\rho_n, \beta_n$  are the states of  $\mathcal{S}$  and  $\mathcal{E}$  for the  $n$ th interaction, respectively. Here,  $U$  is an unitary evolution and  $\mathcal{L}_{\beta_n}$  is called the *reduced dynamics map*, which is a completely positive and trace-preserving (CPTP) map acting on the space  $\mathcal{M}_{\mathcal{S}}$  of density matrices in  $\mathcal{S}$ .

One can ask where the mechanism to obtain the nonlinearity is, since even if the evolution is not unitary we still get linear dynamics. In fact, it has been shown that introducing a coherent nonlinearity to quantum evolution means that we can obtain the ability to solve NP-hard problems [16]. Therefore, a more likely way to introduce nonlinearities is to use projective measurements, which are clearly nonlinear operations using the projectors on the space spanned by the basis of the system used in a measurement. In this way, if a local observable  $O$  is described by a collection of projectors  $\{P_j\}$  as  $O = \sum_j a_j P_j$ , where  $a_j$  are the values of a physical quantity of a measurement associated with  $P_j$ , the probability to obtain the measurement result  $a_j$  is given by  $p(a_j) = \text{Tr}[P_j \rho]$ . Then, the expectation value of the physical quantity is given by

$$a_j p(a_j) = a_j \text{Tr}[P_j \rho] = \text{Tr}[O \rho] = \langle O \rangle_\rho. \quad (\text{S4})$$

We obtain partial information regarding the state  $\rho_n$  of the quantum system  $\mathcal{S}$  after the  $n$ th interaction with the environment by measuring local observables  $O_1, O_2, \dots, O_K$  on the state of  $\mathcal{S}$ . Then, the  $k$ th element  $x_{nk}$  of the reservoir states  $\mathbf{x}_n$  can be calculated as the expectation of the measurement results via  $O_k$  on  $\rho_n$ :

$$x_{nk} = \text{Tr}[O_k \rho_n] = \langle O_k \rangle_{\rho_n}. \quad (\text{S5})$$

One can increase the dimension of  $\mathbf{x}_n$  by performing measurements at multiple times. Between two inputs,  $M$  cycles of the unitary evolution are processed and each of them is followed by a measurement.  $M$  is called the measurement multiplexity. Thus we obtain  $MK$  elements in each reservoir state. After obtaining the reservoir states, the training procedure in QRC is similar to the classical RC.

We note that we can also construct a universal quantum reservoir consisting of multiple and non-interacting quantum reservoirs  $\mathcal{S}$ . For example, let us consider a quantum system  $\mathcal{S}$  consisting of two non-interacting reduced quantum reservoirs  $\mathcal{S}_a$  and  $\mathcal{S}_b$  with the corresponding reduced dynamics maps  $\mathcal{L}_a$  and  $\mathcal{L}_b$ , respectively. Since  $\mathcal{S}_a$  and  $\mathcal{S}_b$  are not interacting, a quantum state  $\rho$  in  $\mathcal{S}$  can be displayed as a tensor product

$$\rho = \rho_a \otimes \rho_b, \quad (\text{S6})$$

where  $\rho_a$  and  $\rho_b$  are two quantum states in  $\mathcal{S}_a$  and  $\mathcal{S}_b$ , respectively. Then, the reduced dynamics map  $\mathcal{L}$  acting on the space  $\mathcal{M}_{\mathcal{S}}$  can be defined as

$$\rho = \rho_a \otimes \rho_b \rightarrow \mathcal{L}(\rho) = \mathcal{L}_a(\rho_a) \otimes \mathcal{L}_b(\rho_b). \quad (\text{S7})$$

## C. Learning the temporal tomography

A significant different in the applications of QRC approaches compared with the conventional RC is the ability to deal with quantum tasks such as the classification of quantum states as entangled or separable [8], the quantum

tomography [9], and the quantum state preparation [10]. While some of the QRC approaches are not proposed for quantum tasks [6, 11, 12], the current proposals of QRC for quantum tasks focused on a static quantum state, which is coupled to the reservoir [8, 9]. Here, our approach based on repeated quantum interactions provides the ability to perform quantum tasks for a sequence of input quantum states where the outputs of these tasks depend on the past input states.

In learning the tomography of the temporal quantum map  $\mathcal{F}$ , we are given an input sequence of states  $\{\beta_1, \dots, \beta_L\}$  and the corresponding target sequence  $\hat{\mathbf{y}} = \{\hat{\mathbf{y}}_1, \dots, \hat{\mathbf{y}}_L\}$ , where  $\hat{\mathbf{y}}_k$  is the real vector form to stack the real and imaginary elements of  $\mathcal{F}(\beta_k)$ . In the evaluation stage, we are given an input sequence  $\{\beta_{L+1}, \dots, \beta_{L+T}\}$  with the corresponding target  $\{\hat{\sigma}_{L+1}, \dots, \hat{\sigma}_{L+T}\}$ , where  $\hat{\sigma}_i = \mathcal{F}(\beta_i)$ . The reconstructed output sequence is  $\{\mathbf{y}_{L+1}, \dots, \mathbf{y}_{L+M}\}$ , which is rearranged in the matrix form  $\{\sigma_{L+1}, \dots, \sigma_{L+T}\}$ . Due to statistical fluctuations, there are some cases in which the reconstructed matrix  $\sigma_i$  is not positive semidefinite. We project  $\sigma_i$  onto the spectrahedron to obtain a positive semidefinite matrix  $\sigma'_i$  such that the trace of  $\sigma'_i$  is equal to 1 and the Frobenius norm between  $\sigma_i$  and  $\sigma'_i$  is minimized [17]. This technique is considered as *projected pseudo-inversion estimator*. Other proposals for a density matrix estimator can be found in a survey in Ref. [18].

## II. CONVERGENCE ANALYSIS

A quantum system with a reproducible temporal information processing ability must produce the trajectories that are robust to small perturbations to the system, i.e., the computations for the same input sequence are independent of its initial state. We refer to this as quantum echo state property (QESP), which is defined in Ref. [19] and mentioned in the convergence property of dissipative quantum systems in Ref. [20].

**Definition S1.** *A quantum system used in temporal information processing tasks is said to satisfy the quantum echo state property (QESP) with respect to the distance  $D$  between quantum states if for any input sequence of length  $L$ , it holds that  $D(\rho_L^{(1)}, \rho_L^{(2)}) \rightarrow 0$  as  $L \rightarrow \infty$ , where  $\rho_L^{(1)}, \rho_L^{(2)}$  are the states after  $L$  steps corresponding with different initial states  $\rho_0^{(1)}, \rho_0^{(2)}$ .*

In the following parts, we consider  $D$  as the trace distance, or the Schatten 1-norm, defined by  $D(\rho, \rho') = \|\rho - \rho'\| = \text{Tr}[\|\rho - \rho'\|]$  between quantum states  $\rho$  and  $\rho'$ , where we define  $|A| = \sqrt{A^\dagger A}$  to be the positive square root of  $A^\dagger A$  for any matrix  $A$ . Since a CPTP map is a contracting map w.r.t. the trace distance, the density matrices in quantum repeated interactions satisfy decreasing system distinguishability [21] as

$$\|\rho_n^{(1)}, \rho_n^{(2)}\| \leq \|\rho_{n-1}^{(1)}, \rho_{n-1}^{(2)}\|, \quad (\text{S8})$$

where  $\rho_n^{(1)}, \rho_n^{(2)}$  are the states after  $n$  interactions corresponding with different initial states  $\rho_0^{(1)}, \rho_0^{(2)}$ . We denote  $\Phi_n = \mathcal{L}_{\beta_n} \mathcal{L}_{\beta_{n-1}} \dots \mathcal{L}_1$ , then  $\Phi_n$  is a CPTP map and  $\rho_n = \Phi_n(\rho_0)$ . We are interested in the action of  $\Phi_n$  to study the dynamics of  $\mathcal{S}$ , particularly in asymptotic behavior in the limit  $n \rightarrow \infty$ .

Since the reduced dynamics maps  $\mathcal{L}_{\beta_n}$  do not have in general a common invariant state, we firstly investigate the behavior of the reservoir at ergodic limits. We use here the results developed in Ref. [22] (Theorem 1.3) and Ref. [23] (Theorem 5.2, Proposition 6.3) to get the following result.

**Result S1** (Ergodicity of the reduced quantum reservoir). *Let  $\{\beta_n\}$  be a sequence of i.i.d. random quantum states under the main hypothesis that the induced CPTP maps  $\mathcal{L}_{\beta_n}$  have a unique invariant state. Then, for all initial states  $\rho_0$ , the reduced quantum reservoir  $\mathcal{S}$  satisfies the ergodic limit*

$$\lim_{N \rightarrow \infty} \frac{1}{N} \sum_{n=1}^N \rho_n = \lim_{N \rightarrow \infty} \frac{1}{N} \Phi_n(\rho_0) = \rho_{\text{es}}, \quad (\text{S9})$$

where  $\rho_{\text{es}} \in \mathcal{M}_{\mathcal{S}}$  is the unique invariant state of the deterministic map  $\mathcal{L}_{\mathbb{E}[\beta]}$ .

Next, motivated by the theory of ergodic quantum processes in Refs. [24, 25], we derive the following theorem as a sufficient condition for the QESP of a QR.

**Result S2.** *The quantum reservoir  $\mathcal{S}$  satisfies the quantum echo state property if the input sequence  $\{\beta_n\}$  is a random ergodic sequence under the main hypothesis that for some  $n$ ,  $\Phi_n$  is a strictly positive CPTP map with a positive probability. Here, a CPTP map  $\mathcal{L} : \mathcal{M}_{\mathcal{S}} \rightarrow \mathcal{M}_{\mathcal{S}}$  is called strictly positive if it sends every positive semidefinite matrix in  $\mathcal{M}_{\mathcal{S}}$  to a positive definite matrix.*

*Proof.*— Since  $\{\beta_n\}$  is an ergodic sequence the sequence of  $\mathcal{L}_{\beta_n}$  is also ergodic. We drop the notion  $\beta$  for an easy description of the reduced dynamics maps  $\mathcal{L}_{\beta_n}$  as  $\mathcal{L}_n$ . We assume that the sequence of  $\mathcal{L}_n$  is drawn from an ensemble  $\Omega$ . Consider the shift map  $\mathcal{T} : \Omega \rightarrow \Omega$  such that  $\mathcal{T}(\mathcal{L}_1, \mathcal{L}_2, \dots) = (\mathcal{L}_2, \mathcal{L}_3, \dots)$ . Due to the ergodic property,  $\mathcal{T}$  is ergodic map, that is, the dynamics generated by  $\mathcal{T}$  starting from a typical sequence will cover  $\Omega$  with full measure. We can write the composition form as

$$\mathcal{L}_{m+n} \dots \mathcal{L}_{m+1} = \mathcal{T}^m \circ \Phi_n, \quad (\text{S10})$$

for any  $n, m \geq 1$ .

For a CPTP map  $\mathcal{L} : \mathcal{M}_S \rightarrow \mathcal{M}_S$ , let  $c(\mathcal{L})$  be the smallest number such that  $\|\mathcal{L}(\rho) - \mathcal{L}(\sigma)\| \leq c(\mathcal{L})\|\rho - \sigma\|$  for any  $\rho, \sigma \in \mathcal{M}_S$ . Because  $\mathcal{L}$  is contracting w.r.t.  $\|\cdot\|$ , such  $c(\mathcal{L})$  always exists and  $0 < c(\mathcal{L}) \leq 1$ . We denote  $c_n = c(\Phi_n)$  and have the following inequalities:

$$c(\Phi_{m+n}) \leq c(\Phi_m)c(\mathcal{L}_{m+n} \dots \mathcal{L}_{m+1}) \quad (\text{S11})$$

$$\ln(c(\Phi_{m+n})) \leq \ln(c(\Phi_m)) + \ln(c(\mathcal{L}_{m+n} \dots \mathcal{L}_{m+1})) \quad (\text{S12})$$

$$\ln(c(\Phi_{m+n})) \leq \ln(c(\Phi_m)) + \ln(c(\mathcal{T}^m \circ \Phi_n)) \quad (\text{S13})$$

As  $\ln(c(\Phi_n)) \leq 0$ , the subadditive ergodic theorem guarantees [26] that the following limit exists:

$$\lim_{n \rightarrow \infty} \frac{1}{n} \ln(c(\Phi_n)) = \kappa, \quad (\text{S14})$$

where  $\kappa \leq 0$  is given by the limit of expectations over  $\Omega$  (Ref. [27], Lemma 3.2)

$$\kappa = \lim_{n \rightarrow \infty} \frac{1}{n} \mathbb{E}[\ln(c(\Phi_n))] = \inf_n \frac{1}{n} \mathbb{E}[\ln(c(\Phi_n))]. \quad (\text{S15})$$

By the hypothesis of the strictly positive map, for some  $n$  we have  $c(\Phi_n) < 1$  with a positive probability. Therefore, there exists  $n \geq 1$  such that  $-\infty \leq \frac{1}{n} \mathbb{E}[\ln(c(\Phi_n))] < 0$ , thus  $\kappa < 0$ . From Eq. (S14), there exists a positive  $\mu < 1$ , a constant  $A > 0$ , and  $n_0 \geq 1$  such that  $c(\Phi_n) \leq A\mu^n$  for all  $n \geq n_0$ . Then,

$$\|\rho_n^{(1)} - \rho_n^{(2)}\| = \|\Phi_n(\rho_0^{(1)}) - \Phi_n(\rho_0^{(2)})\| \leq c(\Phi_n)\|\rho_0^{(1)} - \rho_0^{(2)}\| \leq A\mu^n\|\rho_0^{(1)} - \rho_0^{(2)}\| \quad (\text{S16})$$

for all  $n \geq n_0$ , thus  $\|\rho_n^{(1)} - \rho_n^{(2)}\| \rightarrow 0$  as  $n \rightarrow \infty$ . Therefore, we obtain the QESP. Furthermore, if the system starts from two different states, then the trace distance between the states will decay exponentially to zero.

In some practical situations, result S2 may be too restrictive to be used. We can relax the definition S1 as the following definition.

**Definition S2.** Given a positive  $\varepsilon$ , a quantum reservoir is said to satisfy the  $\varepsilon$ -QESP if for any input sequence there exists a smallest number  $T(\varepsilon)$  such that  $\|\Phi_n(\rho_0^{(1)}) - \Phi_n(\rho_0^{(2)})\| < \varepsilon$  for all  $n \geq T(\varepsilon)$  and all different initial states  $\rho_0^{(1)}, \rho_0^{(2)}$ . The maximum  $T(\varepsilon)$  for all input sequences is defined as the  $\varepsilon$ -QESP time scale of the quantum reservoir.

We demonstrate that the  $\varepsilon$ -QESP and the corresponding time scale can be evaluated via the spectrum of the reduced dynamic maps  $\mathcal{L}_n$ . First, we consider the case of the constant input  $\beta_n = \beta$  for all  $n$ . We have  $\mathcal{L}_n \equiv \mathcal{L}$  for all  $n$  and  $\rho_n = \mathcal{L}^n(\rho_0)$ . Any density matrix can be converted into the vector form, which allows us to define a linear space of matrices (Fock-Liouville space) associated with an inner product. Consider an arbitrary density matrix  $\rho = \sum_{i,j} \rho_{i,j} |i\rangle \langle j|$ . We can write its vectorized form using the Choi-Jamiolkowski isomorphism as  $\text{vec}(\rho) = \sum_{i,j} \rho_{i,j} |j\rangle \otimes |i\rangle$ , which is the same as stacking columns of  $\rho$ . The reduced dynamics map  $\mathcal{L}$  can now be expressed as a matrix  $\tilde{\mathcal{L}}$ , such that  $\text{vec}(\rho_n) = \tilde{\mathcal{L}} \text{vec}(\rho_{n-1})$ . The spectrum of  $\mathcal{L}$  can be written as  $1 = |\lambda_1| \geq |\lambda_2| \geq \dots \geq |\lambda_s|$ , where  $\lambda_j$  is the  $j$ th eigenvalue of  $\tilde{\mathcal{L}}$ . Because  $\mathcal{L}$  can be a non-Hermitian map, it can have both left and right eigenmatrices. We denote  $L_j$  and  $R_j$  as the left and right eigenmatrices corresponding to eigenvalue  $\lambda_j$ , respectively. We choose the normalization such that  $\text{Tr}(L_k R_l) = \delta_{kl}$  for all  $1 \leq k, l \leq s$ , and  $\text{Tr}[R_1] = 1$  (i.e.,  $L_1$  being the identity  $L_1 = I$ ). Since  $\text{vec}(\rho_n) = \tilde{\mathcal{L}}^n(\text{vec}(\rho_0))$ , we have

$$\text{vec}(\rho_n) = \text{vec}(R_1) + \sum_{j=2}^s b_j \lambda_j^n \text{vec}(R_j), \quad (\text{S17})$$

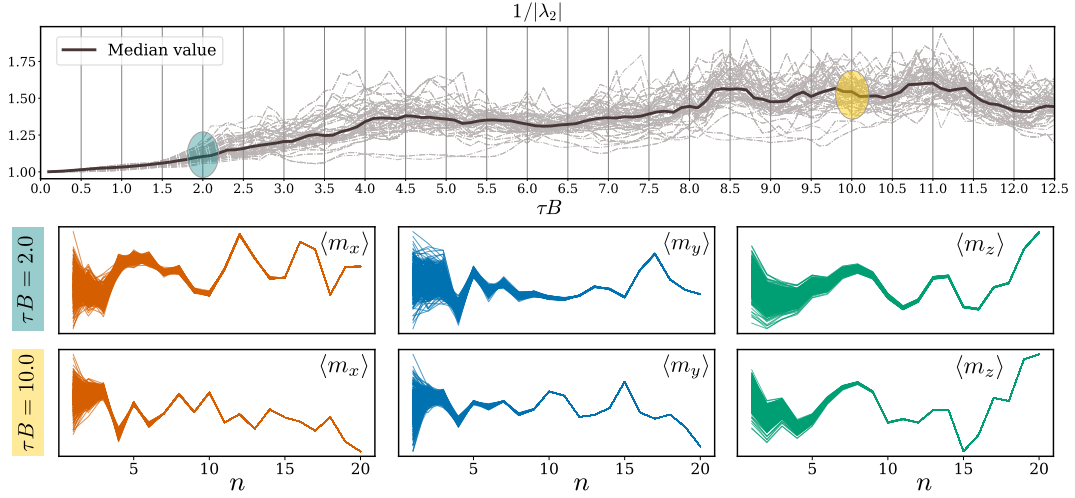


FIG. S1. (Top) The values of  $1/|\lambda_2|$  for 100 random reduced dynamics maps  $\mathcal{L}_\beta$  with  $N_m = 4, N_e = 2, \alpha = 1, J = 1$ , and  $J/B = 1$ . The solid line depicts the median value of the ensemble of dynamics maps. (Middle and bottom) The trajectories of the average magnetization generated with 500 random initial states of  $\mathcal{S}$  at  $\tau B = 2.0$  and  $\tau B = 10.0$ .

where  $b_j = \text{vec}(L_j)^\dagger \text{vec}(\rho_0) = \text{Tr}[L_j \rho_0]$ . Therefore, if  $|\lambda_2|^{-1} > 1$ , the steady state  $\rho_{\text{ss}}$  of the system is unique ( $\rho_{\text{ss}} = R_1$ ) with the convergence rate depending on the magnitude of  $|\lambda_2|^{-1}$ , i.e.,  $\|\rho_n - \rho_{\text{ss}}\| \sim e^{-n/N}$  with  $N \sim \frac{1}{\ln(|\lambda_2|^{-1})}$ . The QESP is satisfied that we can evaluate the  $\varepsilon$ -QESP time scale as  $O(\frac{\ln(\varepsilon^{-1})}{\ln(|\lambda_2|^{-1})})$ .

Next, we consider the case when the input is a sequence of i.i.d. density matrices. The result S2 provides us the following proposition, which is stated in our main text.

**Proposition S1.** *If there exist  $n_0$  such that  $\mu = \max(c_n) < 1$  for all  $n \geq n_0$ , where  $0 < c_n \leq 1$  is the contraction coefficient of  $\mathcal{L}_{\beta_n}$ , then the  $\varepsilon$ -QESP time scale can be evaluated as  $O(\frac{\ln(\varepsilon^{-1})}{\ln(\mu^{-1})})$ .*

*Proof.*— In the proof of result S2, for a CPTP map  $\mathcal{L} : \mathcal{M}_{\mathcal{S}} \rightarrow \mathcal{M}_{\mathcal{S}}$ , the contraction coefficient  $c(\mathcal{L})$  denotes the smallest number such that  $\|\mathcal{L}(\rho) - \mathcal{L}(\sigma)\| \leq c(\mathcal{L})\|\rho - \sigma\|$  for any  $\rho, \sigma \in \mathcal{M}_{\mathcal{S}}$ . Such  $c(\mathcal{L})$  always exists and  $0 < c(\mathcal{L}) \leq 1$ . Since  $\mu = \max(c_n) < 1$  for all  $n \geq n_0$ , we have  $c(\Phi_n) \leq A\mu^n < 1$  for some constant  $A$  for all  $n \geq n_1 \geq n_0$  for some  $n_1$ . Equation (S16) shows us the result in the proposition.

Proposition S1 gives us a consequence that to obtain a sufficient check for the QESP and to know the  $\varepsilon$ -QESP time scale, we only need to investigate the contracting coefficient via the spectrum of the reduced dynamics map for random input.

To numerically investigate the transient dynamics, we consider a specific system modeled by the transverse field Ising model, where the Hamiltonian is given by

$$H = - \sum_{i>j=1}^N J_{i,j} \hat{s}_i^x \hat{s}_j^x - B \sum_j^N \hat{s}_j^z. \quad (\text{S18})$$

Here,  $B$  is the natural frequency of 1/2-spins represented for qubits.  $\hat{s}_j^\gamma$  ( $\gamma \in \{x, y, z\}$ ) are the Pauli operators measuring the qubit  $j$  along the  $\gamma$  direction, which can be described as an  $N$ -tensor product of  $2 \times 2$ -matrices as

$$\hat{s}_j^\gamma = \mathbf{I} \otimes \dots \otimes \underbrace{\hat{s}^\gamma}_{j\text{-index}} \otimes \dots \otimes \mathbf{I}, \quad (\text{S19})$$

where  $\mathbf{I} = \begin{bmatrix} 1 & 0 \\ 0 & 1 \end{bmatrix}$ ,  $\hat{s}^x = \begin{bmatrix} 0 & 1 \\ 1 & 0 \end{bmatrix}$ ,  $\hat{s}^y = \begin{bmatrix} 0 & -i \\ i & 0 \end{bmatrix}$ , and  $\hat{s}^z = \begin{bmatrix} 1 & 0 \\ 0 & -1 \end{bmatrix}$ . The coupling coefficients  $J_{ij}$  between spins can be randomly selected or fixed depending on the distance of interaction. To describe our QR, we assume that the auxiliary system  $\mathcal{E}$  includes the first  $N_e$  spins where the remaining  $N_m = N - N_e$  spins form the reservoir  $\mathcal{S}$ . We present the setting of *power-law decaying* for  $J_{ij}$  and frequency  $B$  corresponding with the physical implementation in a trapped-ion quantum simulation [28–30]. Here,  $J_{ij} = J|i - j|^{-\alpha}/N(\alpha)$  with an interaction strength  $J$ , power coefficient  $0 < \alpha < 3$ , and normalization constant  $N(\alpha) = \frac{1}{N-1} \sum_{i>j} |i - j|^{-\alpha}$ . The coupled system  $(\mathcal{S}, \mathcal{E})$  is a

closed system with the total Hamiltonian  $H$  unchanged during each interaction. We consider the model parameters  $\alpha = 1, J = 1, J/B = 1$ , and the unitary  $U = \exp(-i\tau H)$ , where  $\tau$  is the interaction time.

The top panel of Fig. S1 shows the values of  $1/|\lambda_2|$  according to the normalized interaction time  $\tau B$  for 100 random reduced dynamics maps  $\mathcal{L}_\beta(\rho) = \text{Tr}_\mathcal{E}[U(\rho \otimes \beta)U^\dagger]$  with  $N_m = 4, N_e = 2$ . Here,  $\beta$  is drawn from an ensemble of Haar random pure states of dimension  $2^{N_e}$ . The QESP is satisfied in values of  $\tau B$  such as all values of  $1/|\lambda_2|$  are higher than 1. Furthermore, the higher  $1/|\lambda_2|$  leads to the smaller  $\varepsilon$ -QESP time scale. We then fix a random input sequence and investigate the trajectories of the average magnetization  $\langle m_\gamma \rangle = \text{Tr}[\hat{m}_\gamma \rho_n]$ , where  $\hat{m}_\gamma = \frac{1}{N_m} \sum_j \hat{s}_j^\gamma$  are the average spin operators at  $\gamma \in \{x, y, z\}$  directions in  $\mathcal{S}$ . The trajectories begin with 500 random initial states of  $\mathcal{S}$ . The fluctuations reduce as the number  $n$  of interactions increases. This reduction is faster as the  $\varepsilon$ -QESP scale is smaller, as illustrated in Fig. S1 with  $\tau B = 2.0$  and  $\tau B = 10.0$ .

### III. METASTABILITY ANALYSIS

In this section, we derive the metastability of the reservoir dynamics. Metastability is a characteristic feature of the dynamics of a slow relaxing system with the partial relaxation into long-lived states before eventual decay to the true stationary state. Metastability appears due to the separation of time scales in the dynamics; therefore, different initial states of the system will relax to different metastable states in the transient dynamics before eventual relaxation to the true stationary state. The metastability in open quantum systems has been studied in Ref. [31]. Here, we formulate the metastability in our quantum reservoir framework.

First, we consider the case of constant input  $\beta_n = \beta$  for all  $n$ . The reduced dynamic map is represented by a fixed CPTP map  $\mathcal{L}$  with the spectrum  $1 = |\lambda_1| \geq |\lambda_2| \geq \dots |\lambda_s|$ , where  $\lambda_j$  is the  $j$ th eigenvalue of  $\mathcal{L}$ . We observe that each  $\lambda_j$  such that  $|\lambda_j| < 1$  represents a time scale of the system. Let us assume that  $|\lambda_2| < 1$  and there is a large separation between  $|\lambda_m|$  and  $|\lambda_{m+1}|$  in the spectrum of  $\mathcal{L}$  as  $1 = |\lambda_1| \geq \dots |\lambda_m| \gg |\lambda_{m+1}| \geq \dots |\lambda_s|$ . This separation corresponds to two scales defined by  $N_1 = \frac{1}{\ln(|\lambda_{m+1}|^{-1})}$  and  $N_2 = \frac{1}{\ln(|\lambda_m|^{-1})}$ . The range  $N_1 \ll n \ll N_2$  defines the range where the metastability occurs and the system relaxes into a state in metastable manifold (MM), which we can consider as an effective dimensional reduction. In the metastable regime, the dynamics will be described via the motion in the MM towards the true stationary state, which is reached at  $n \gg N_2$ .

The MM is a convex subset of the system states on which the long-time dynamics takes place. From Eq. (S17), the projection  $\mathcal{P}$  of  $\rho_n$  onto the MM is given by

$$\mathcal{P}\rho_n = \rho_{\text{ss}} + \sum_{j=2}^m \text{Tr}[\rho_n L_j] R_j. \quad (\text{S20})$$

The evolution of dynamics in this MM is described by the effective reduced dynamic map  $\mathcal{L}_{\text{eff}} = \mathcal{P}\mathcal{L}\mathcal{P}$ , which is the projection of  $\mathcal{L}$  on the MM. In this sense, MM can be regarded as being  $(m-1)$  dimensional simplex, but each point in this manifold represents a density matrix in  $\mathcal{M}_\mathcal{S}$ . The general structure for MM is discussed in Ref. [31], where MM is determined by a subset in  $\mathbb{R}^{m-1}$  given by the coefficients bounded by the maximum and minimum eigenvalues of the relevant left eigenmatrices  $L_j$  for  $1 \leq j \leq m$ .

From the perspective in temporal processing of the quantum reservoir, the higher-dimensional the MM the longer effects of the reservoir's initial states remained in the processing stream to hamper the QESP. In contrast, if the dynamics is characterized in a low-dimensional MM, the effects of the initial states are reduced faster and the local observables are remained in a relaxation behavior, which are favorable for the QESP.

To understand the transient dynamics, we consider a specific case when the large separation occurs at  $m = 2$ . Here, the MM is a one-dimensional simplex, and the metastable states for this case can be considered as a linear combination of the states at end points of the MM, which are called *extreme metastable states* (EMSs) [31]. These EMSs are defined as follows:

$$\tilde{\rho}_1 = \rho_{\text{ss}} + v_2^{\text{max}} R_2, \quad \tilde{\rho}_2 = \rho_{\text{ss}} + v_2^{\text{min}} R_2, \quad (\text{S21})$$

where  $v_2^{\text{max}}$  and  $v_2^{\text{min}}$  are the maximal and minimal eigenvalues of  $L_2$ , which are real numbers since  $L_2$  is a Hermitian matrix. Because  $L_2$  and  $\rho_{\text{ss}}$  are different eigenmodes of  $\mathcal{L}$ , we obtain the orthogonality as  $\text{Tr}[L_2 \rho_{\text{ss}}] = 0$ . From Lemma II.1 in Ref. [32] and since  $L_2$  is a Hermitian matrix and  $\rho_{\text{ss}}$  is a Hermitian and positive semi-definite matrix, we obtain the following inequality:

$$v_2^{\text{min}} \text{Tr}[\rho_{\text{ss}}] \leq \text{Tr}[L_2 \rho_{\text{ss}}] \leq v_2^{\text{max}} \text{Tr}[\rho_{\text{ss}}]. \quad (\text{S22})$$

Because  $\text{Tr}[\rho_{\text{ss}}] = 1$  and  $L_2$  is not a zero matrix, we have  $v_2^{\text{min}} \leq 0$ ,  $v_2^{\text{max}} \geq 0$ , and  $v_2^{\text{max}} - v_2^{\text{min}} > 0$ .



The projection of a quantum state  $\rho$  onto the MM is a linear combination of the extreme metastable states as

$$\mathcal{P}\rho = p^{(1)}\tilde{\rho}_1 + p^{(2)}\tilde{\rho}_2, \quad (\text{S23})$$

where  $p^{(1,2)} = \text{Tr}[P_{1,2}\rho]$ , and  $P_{1,2}$  are the matrices defined by

$$P_1 = \frac{L_2 - v_2^{\min}I}{\Delta v_2} \quad \text{and} \quad P_2 = \frac{-L_2 + v_2^{\max}I}{\Delta v_2}, \quad (\text{S24})$$

where  $\Delta v_2 = v_2^{\max} - v_2^{\min}$ . These matrices satisfy  $P_{1,2} \geq 0$  and  $P_1 + P_2 = I$ . Therefore  $P_{1,2}$  constitute a POVM. Furthermore, the EMSs  $\tilde{\rho}_1$  and  $\tilde{\rho}_2$  are approximately disjoint (see Supplemental Material in Ref. [31]).

As the number of interactions  $n \gg N_1$ , the quantum reservoir dynamics can be captured by the effective long-time dynamics in the MM. The reservoir state corresponding with the measurement of an observable  $O$  after the  $n$ th interaction can be calculated as

$$\langle O \rangle_{\rho_n} = \sum_i p_n^{(i)} \text{Tr}[O\tilde{\rho}_i]. \quad (\text{S25})$$

In our quantum reservoir, the projection of  $\rho_n$  after the  $n$ th interaction is

$$\mathcal{P}\rho_n = p_n^{(1)}\tilde{\rho}_1 + p_n^{(2)}\tilde{\rho}_2. \quad (\text{S26})$$

We can project both the left and right side of the formula  $\rho_{n+1} = \mathcal{L}(\rho_n)$  to the MM and obtain

$$p_{n+1}^{(1)}\tilde{\rho}_1 + p_{n+1}^{(2)}\tilde{\rho}_2 = p_n^{(1)}\mathcal{L}(\tilde{\rho}_1) + p_n^{(2)}\mathcal{L}(\tilde{\rho}_2). \quad (\text{S27})$$

Since  $\lambda_2$  is the eigenvalue of  $\tilde{\mathcal{L}}$  with the corresponding right eigenmatrix  $R_2$ , we have

$$\begin{aligned} \mathcal{L}(\tilde{\rho}_1) &= \rho_{\text{ss}} + v_2^{\max}\lambda_2 R_2 = \lambda_2\tilde{\rho}_1 + (1 - \lambda_2)\rho_{\text{ss}} \\ &= \frac{1}{\Delta v_2} \{ [\lambda_2 v_2^{\max} - v_2^{\min}] \tilde{\rho}_1 + (1 - \lambda_2) v_2^{\max} \tilde{\rho}_2 \}, \end{aligned} \quad (\text{S28})$$

$$\begin{aligned} \mathcal{L}(\tilde{\rho}_2) &= \rho_{\text{ss}} + v_2^{\min}\lambda_2 R_2 = \lambda_2\tilde{\rho}_2 + (1 - \lambda_2)\rho_{\text{ss}} \\ &= \frac{1}{\Delta v_2} \{ (1 - \lambda_2) v_2^{\min} \tilde{\rho}_1 + [v_2^{\max} - \lambda_2 v_2^{\min}] \tilde{\rho}_2 \}. \end{aligned} \quad (\text{S29})$$

From Eqs. (S26)–(S29), the evolution dynamics on the MM can be described by the dynamics of  $\mathbf{p}_n = \begin{bmatrix} p_n^{(1)} \\ p_n^{(2)} \end{bmatrix}$  as

$$\mathbf{p}_{n+1} = \frac{1}{\Delta v_2} \begin{bmatrix} \lambda_2 v_2^{\max} - v_2^{\min} & -(1 - \lambda_2) v_2^{\min} \\ (1 - \lambda_2) v_2^{\max} & v_2^{\max} - \lambda_2 v_2^{\min} \end{bmatrix} \mathbf{p}_n, \quad (\text{S30})$$

or

$$\Delta \mathbf{p}_n = \mathbf{p}_{n+1} - \mathbf{p}_n = A_{\text{eff}} \mathbf{p}_n, \quad (\text{S31})$$

where

$$A_{\text{eff}} = \frac{1 - \lambda_2}{\Delta v_2} \begin{bmatrix} -v_2^{\max} & -v_2^{\min} \\ v_2^{\max} & v_2^{\min} \end{bmatrix}. \quad (\text{S32})$$

Because  $v_2^{\max} \geq 0$  and  $v_2^{\min} \leq 0$  are real numbers, from Eq. (S31) we note that  $\lambda_2$  must be real. Furthermore, since we assume that  $|\lambda_2| < 1$ , the matrix  $A_{\text{eff}}$  has non-positive diagonal terms and non-negative off-diagonal terms. The sum of entries in each column in  $A_{\text{eff}}$  is equal to 0. Therefore,  $A_{\text{eff}}$  can be considered as a generator of a discrete-time Markov chain induced from states in the MM. This generator describes the classical stochastic dynamics between two metastable states  $\tilde{\rho}_1$  and  $\tilde{\rho}_2$ , and for  $n \rightarrow \infty$  we obtain the probabilities corresponding to the stationary state  $\rho_{\text{ss}}$ .

In the numerical analysis with the model in Eq. (S18), we further investigate the eigenvalues' distribution of the reduced dynamics map  $\mathcal{L}_\beta$ . We first measure the ratios in absolute values between two consecutive eigenvalues as  $r_k = |\lambda_{k+1}|/|\lambda_k|$ , which indicates the separation of time scales in the dynamics. In Fig. S2(a), the top panel shows the

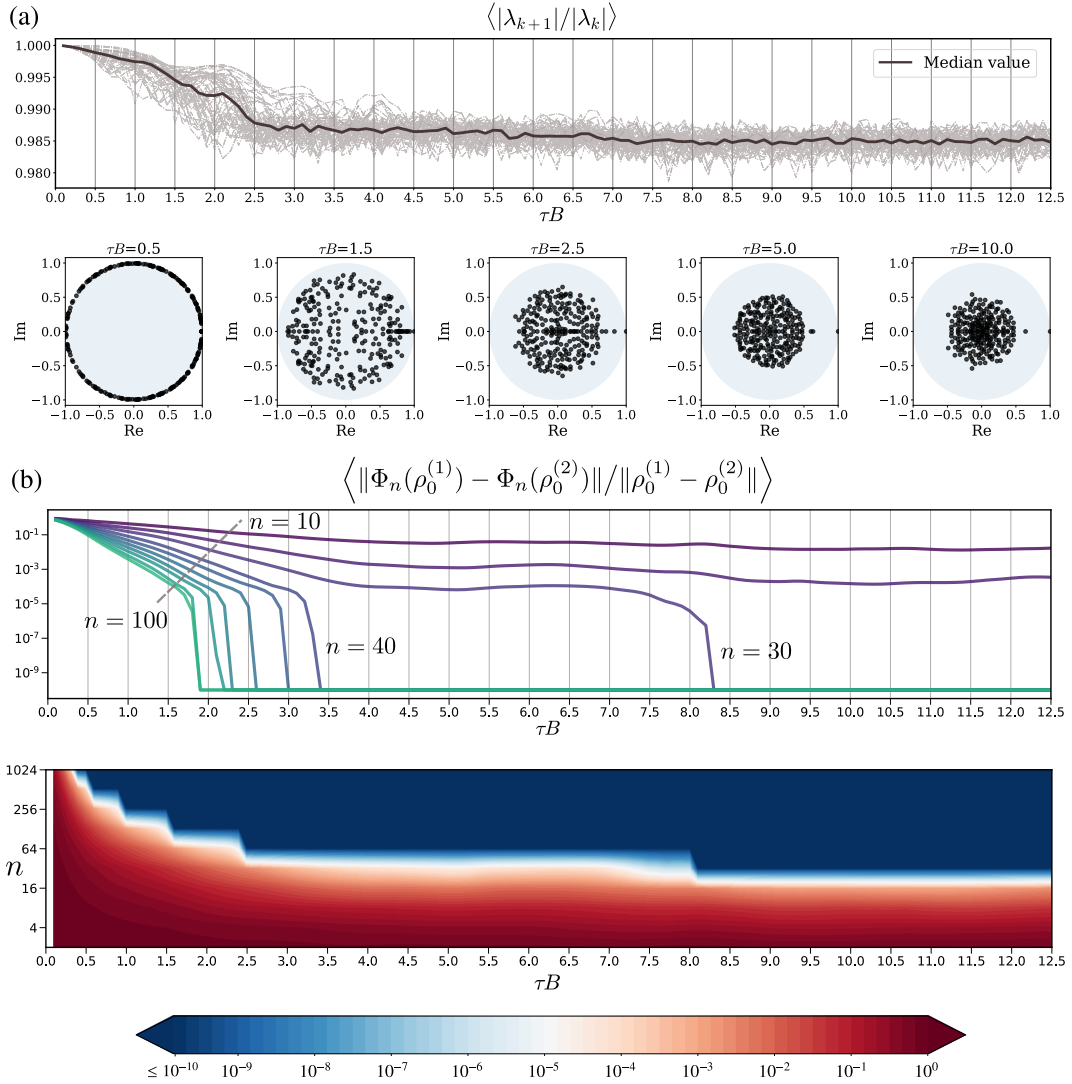


FIG. S2. (a) (Top) The values of  $\langle |\lambda_{k+1}|/|\lambda_k| \rangle$  for 100 random reduced dynamics maps  $\mathcal{L}_\beta$  with  $N_m = 4$ ,  $N_e = 2$ ,  $\alpha = 1$ ,  $J = 1$  and  $J/B = 1$ . The solid line depicts the median value of the ensemble of dynamics maps. (Bottom) The distribution of eigenvalues in the unit disk at  $\tau B = 0.5, 1.5, 2.5, 5.0, 10.0$ . (b) (Top) The distance ratio between the trace distance of final states  $\Phi_n(\rho_0^{(1)}), \Phi_n(\rho_0^{(2)})$  and the trace distance of initial states  $\rho_0^{(1)}, \rho_0^{(2)}$  for the number of interaction steps going from  $n = 10$  (purple line),  $n = 20, 30, \dots$  to  $n = 100$  (green line). This ratio is averaged over 100 different pairs of initial states keeping  $\|\rho_0^{(1)} - \rho_0^{(2)}\| > 0.5$ . All values below the threshold of  $10^{-10}$  are kept to this minimum value for clear visualization. (Bottom) The distance ratio as the function of  $\tau B$  and  $n$ . The levels of the ratio are indicated by the color bar.

expectation value of  $r_k$  over  $k$  according to the normalized time  $\tau B$  for 100 random  $\mathcal{L}_\beta$  with  $N_m = 4$ ,  $N_e = 2$ . The bottom panel of Fig. S2(a) displays exemplary distributions of eigenvalues for  $\tau B = 0.5, 1.5, 2.5, 5.0, 10.0$ . To examine the convergence property, in the top panel of Fig. S2(b), we plot the distance ratio between the trace distance of final states  $\Phi_n(\rho_0^{(1)}), \Phi_n(\rho_0^{(2)})$  and the trace distance of initial states  $\rho_0^{(1)}, \rho_0^{(2)}$  for the number of interaction steps going from  $n = 10$  (purple line),  $n = 20, 30, \dots$  to  $n = 100$  (green line). This ratio is averaged over 100 different pairs of initial states maintaining  $\|\rho_0^{(1)} - \rho_0^{(2)}\| > 0.5$ . In the bottom panel of Fig. S2(b), the calculated ratios are displayed as the function of  $\tau B$  and the number  $n$  of interactions, where the color bar indicates the levels of ratios.

If the eigenvalues are close to the unit border or  $r_k$  are close to 1,  $\mathcal{L}_\beta$  reduces toward a unitary map and the QR relaxes into a state on a high-dimensional MM. Such long-time dynamics makes the QR retain the information of its initial states on the MM. We observe the transition ( $1.5 \leq \tau B \leq 2.5$ ) from high values to a stable range of  $\langle r_k \rangle$ . In the stable range, more eigenvalues are moved near the center of the unit disk, the effects of initial states are reduced, and the dynamics will be characterized by lower-dimensional MMs in a more ergodic phase. As demonstrated in the bottom panel of Fig. S2(b), the convergence property is also enhanced in this phase.

#### IV. QUANTUM SHORT-TERM MEMORY CAPACITY

The capacity to reconstruct the previous  $d$  steps of the input states is evaluated via the square of the distance correlation [33] between the output  $\{\sigma_n\}$  and the target  $\{\hat{\sigma}_n\} = \{\beta_{n-d}\}$ :

$$\mathcal{R}^2(d) = \frac{\mathcal{V}^2(\{\sigma_n\}, \{\hat{\sigma}_n\})}{\mathcal{V}(\{\sigma_n\})\mathcal{V}(\{\hat{\sigma}_n\})}. \quad (\text{S33})$$

Here,  $\mathcal{V}(\{\rho_n\}, \{\sigma_n\})$  and  $\mathcal{V}(\{\rho_n\}) = \mathcal{V}(\{\rho_n\}, \{\rho_n\})$  represent the distance covariance and distance standard deviation of random sequences of density matrices  $\{\rho_n\}, \{\sigma_n\}$ .

The distance covariance  $\mathcal{V}(\{\rho_n\}, \{\sigma_n\})$  is calculated from all pairwise distances  $A(\rho_j, \rho_k)$  and  $A(\sigma_j, \sigma_k)$  for  $j, k = 1, 2, \dots, n$ . Here, the distance  $A(\rho, \sigma) = \arccos F(\rho, \sigma)$  for given density matrices  $\rho$  and  $\sigma$  is defined as the angle induced from the fidelity  $F(\rho, \sigma) = \left(\text{Tr}[\sqrt{\sqrt{\sigma}\rho\sqrt{\sigma}}]\right)^2$ . We construct the distance matrices for  $\{\rho_n\}$  and  $\{\sigma_n\}$  as  $(R_{jk})$  and  $(S_{jk})$  with the elements  $R_{jk} = A(\rho_j, \rho_k)$  and  $S_{jk} = A(\sigma_j, \sigma_k)$ . We take all double centered distances

$$r_{j,k} = R_{j,k} - \bar{R}_{j.} - \bar{R}_{.k} + \bar{R}_{..}, \quad (\text{S34})$$

$$s_{j,k} = S_{j,k} - \bar{S}_{j.} - \bar{S}_{.k} + \bar{S}_{..}, \quad (\text{S35})$$

where  $\bar{R}_{j.}$  and  $\bar{R}_{.k}$  are the  $j$ th row mean and the  $k$ th column mean, respectively, and  $\bar{R}_{..}$  is the grand mean of the distance matrix  $(R_{jk})$  (the same notations for  $S$ ). The squared distance covariance is the arithmetic average of the products  $r_{j,k}s_{j,k}$

$$\mathcal{V}^2(\{\rho_n\}, \{\sigma_n\}) = \frac{1}{n^2} \sum_{j=1}^n \sum_{k=1}^n r_{j,k}s_{j,k}. \quad (\text{S36})$$

The distance covariance and correlation are developed for measuring the dependence and testing independence between two random vectors [33]. In the definition of  $\mathcal{R}^2(d)$ , we are interested in the empirical distance covariance and correlation to study the serial dependence between  $\{\sigma_n\}$  and  $\{\hat{\sigma}_n\} = \{\beta_{n-d}\}$ . Here,  $0 \leq \mathcal{R}^2(d) \leq 1$ , and  $\mathcal{R}^2(d) = 1$  if we can find some linear transformation from the output sequence  $\{\sigma_n\}$  to the target sequence  $\{\hat{\sigma}_n\}$ . In contrast,  $\mathcal{R}^2(d) = 0$  implies that the system cannot reconstruct the previous  $d$  steps of the inputs because the output and the target sequences are completely independent. We define  $\mathcal{R}^2(d)$  as the *quantum short-term memory function* of the quantum reservoir to represent the fraction of distance variance explainable in a sequence of states by other. We then define the *quantum short-term memory capacity* as  $\text{QMC} = \sum_{d=0}^{\infty} \mathcal{R}^2(d)$  to measure how much distance variance of the delay input states can be recovered from reconstructed output states, summed over all delays.

The QMC is motivated from the short-term memory capacity in classical reservoir computing [34] and is generally proposed here as a standard quantity to compare the temporal processing capacity of quantum devices. We note that without the condition of the quantum states,  $\sigma_n$  and  $\hat{\sigma}_n$  can be written in the vector form, and the QMC can be defined in a same way with the classical short-term memory capacity in Ref. [1] and Definition 1 in Ref. [35]. In this situation, the QMC is bounded by the number of elements ( $MK$ ) in each reservoir state if the input states are i.i.d. We hypothesize that this bound is still true for the definition of  $\mathcal{R}^2(d)$  and QMC in our framework. The numerical results in Fig. S3, Fig. S5 and Fig. S6 are already sound the way they are. In these numerical simulations, the first 1000 time steps are excluded for initial transients to satisfy the QESP. The training and evaluating are performed with 3000 and 100 time steps, respectively. The capacity is averaged over ten random trials of input sequences and initial states.

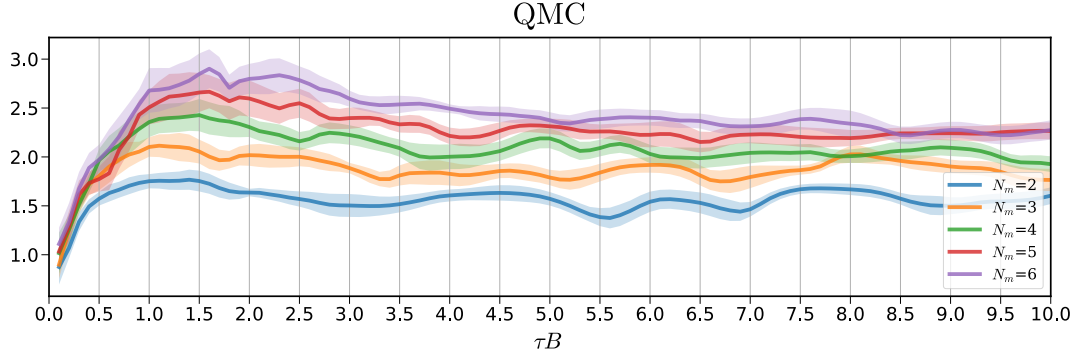


FIG. S3. Quantum short-term memory capacity (QMC) for sequences of i.i.d. two-qubit states of the quantum reservoir modeled in Eq. (S18) according to the normalized interaction time  $\tau B$  and the number  $N_m$  of qubits in the reservoir. Other model parameters are  $\alpha = 1.0$ ,  $J = 1.0$ , and  $J/B = 1.0$ . The QMC is calculated until  $d_{\max} = 20$ . The lines depict the average QMC across 10 sequences of i.i.d. input states. The shaded areas indicate the confidence intervals (one standard deviation) calculated in the same ensemble of runs.

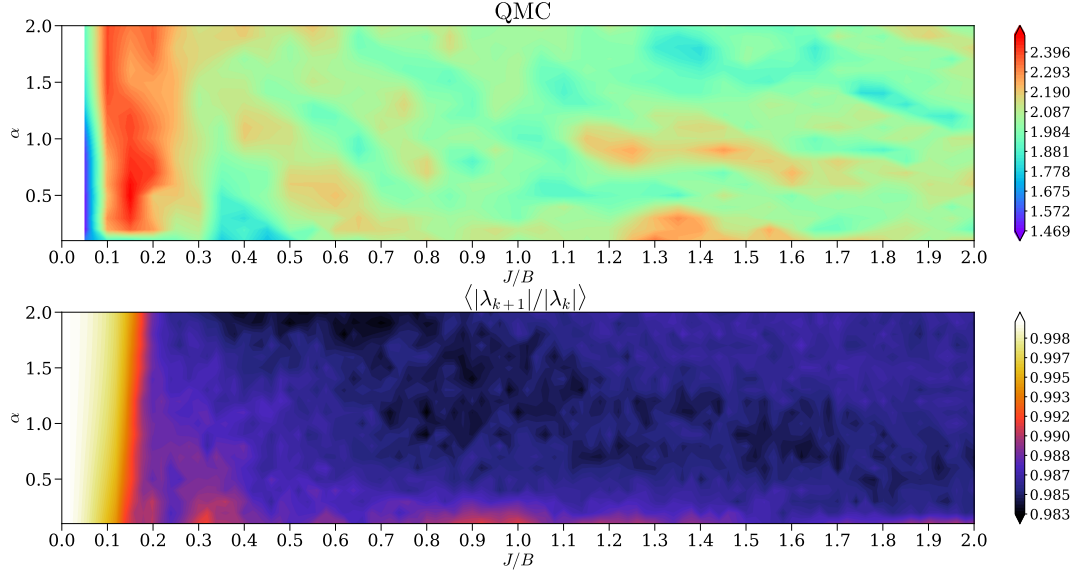


FIG. S4. (Top) Quantum short-term memory capacity (calculated until  $d_{\max} = 10$ ) as the function of model parameters  $\alpha$  and  $J/B$  with  $N_e = 2$ ,  $N_m = 4$ , and  $\tau B = 10.0$ . (Bottom) The value  $\langle |\lambda_{k+1}|/|\lambda_k| \rangle$  over  $k$  as the function of model parameters.

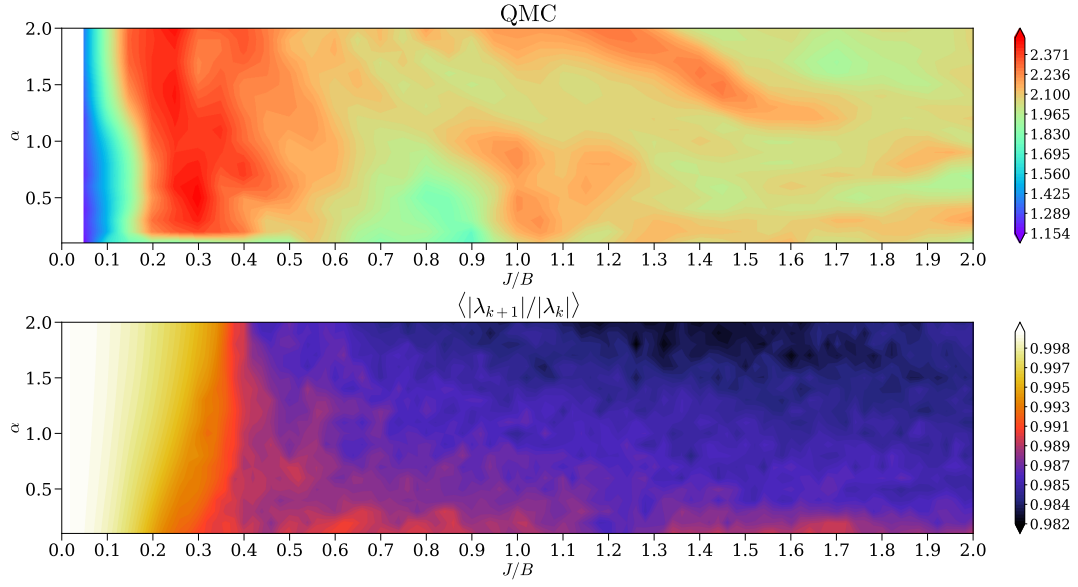


FIG. S5. (Top) Quantum short-term memory capacity (calculated until  $d_{\max} = 10$ ) as the function of model parameters  $\alpha$  and  $J/B$  with  $N_e = 2$ ,  $N_m = 4$ , and  $\tau B = 5.0$ . (Bottom) The value  $\langle |\lambda_{k+1}|/|\lambda_k| \rangle$  over  $k$  as the function of model parameters.

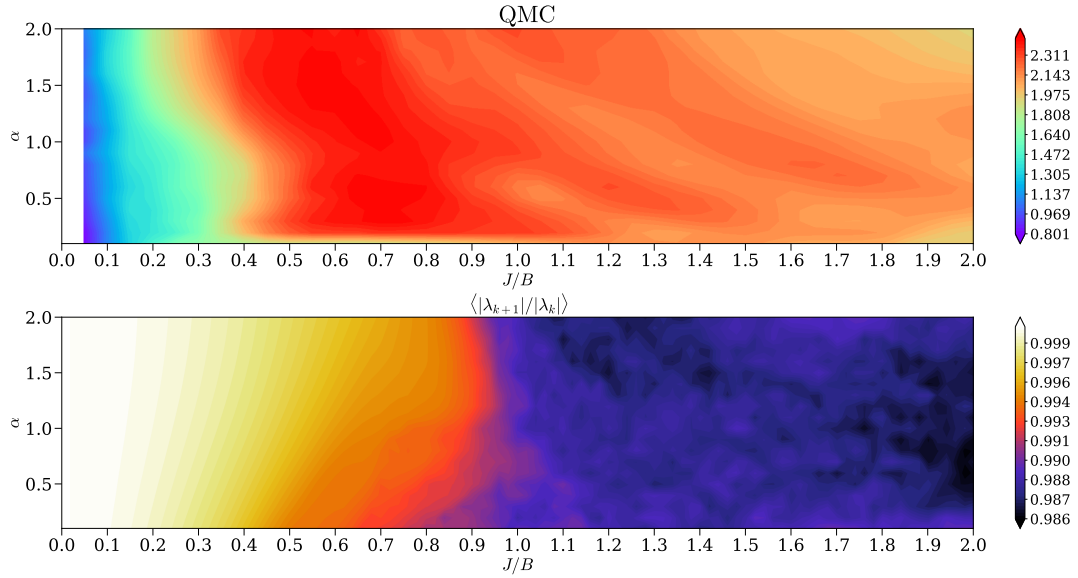


FIG. S6. (Top) Quantum short-term memory capacity (calculated until  $d_{\max} = 10$ ) as the function of model parameters  $\alpha$  and  $J/B$  with  $N_e = 2$ ,  $N_m = 4$ , and  $\tau B = 2.0$ . (Bottom) The value  $\langle |\lambda_{k+1}|/|\lambda_k| \rangle$  over  $k$  as the function of model parameters.



## V. RESULTS ON THE TEMPORAL TOMOGRAPHY TASKS

Given a sequence of input states  $\beta_1, \beta_2, \dots$  in a Hilbert space  $\mathcal{H}_A$  with the dimension  $D_A$ , we consider the temporal map  $\mathcal{F}$  as

$$\mathcal{F}(\beta_n) = \frac{1}{Z} \sum_{i=0}^d \eta_i \Omega_{n-i}(\beta_{n-i}), \quad (\text{S37})$$

where  $\Omega_1, \Omega_2, \dots$  is a sequence of unknown quantum channels from  $\mathcal{H}_A$  to another Hilbert space, and  $\eta_i$  are unknown non-negative real numbers with  $Z = \sum_{i=0}^d \eta_i$  to preserve the trace. Our objective is to characterize  $\mathcal{F}$  from the measurement data. If  $\eta_i = 1$  for all  $i$ , we can consider  $\mathcal{F}$  as a quantum version of the simple moving average filter for a sequence of quantum channels  $\Omega_1, \Omega_2, \dots$  acting on the input states. If  $\eta_i = (d+1-i)$  for all  $i$ , we have a weighted moving average filter. If  $\eta_d = 1$  and  $\eta_i = 0$  for  $i \neq d$ , we have a memory-based reconstruction of the channel applied on  $d$ -delay quantum states. In our demonstration, we set  $\Omega_n$  as a time-dependent depolarizing quantum channel  $\Omega_n(\beta) = p_n \frac{I}{D} + (1-p_n)\beta$ . The depolarizing probability  $p_n$  is formulated as the  $r$ th-order nonlinear dynamical output  $p_n = \kappa p_{n-1} + \eta p_{n-1} \left( \sum_{j=0}^{r-1} p_{n-j-1} \right) + \gamma u_{n-r+1} u_n + \delta$ , where  $r = 10, \kappa = 0.3, \eta = 0.04, \gamma = 1.5$ , and  $\delta = 0.1$ . Here,  $\{u_n\}$  is a random sequence of scalar values in  $[0, 0.2]$  to set  $p_n$  into the stable range in  $[0, 1]$ . The sequence  $\{p_n\}$  resembles the NARMA benchmark [36], which is commonly used for evaluating the computational capability of temporal processing with long time dependence. This setting makes the quantum channel  $\Omega_n$  dependent on to the previous channels, then the tomography task requires memory to characterize these channels.

Figure S7 illustrates an example of a memory-based reconstruction of the quantum channel ( $\eta_d = 1$  and  $\eta_i = 0$  for  $i \neq d$ ) with delay time  $d = 5, N_m = 5, N_e = 1$ , and the measurement multiplexity  $M = 1, 5$ . Other model parameters are  $\alpha = 1.0, J/B = 1.0$ . Here, the first  $t_{\text{buffer}} = 500$  time steps are excluded for initial transients to satisfy the QESP. The training and evaluating are performed in the range  $(t_{\text{buffer}}, t_{\text{train}}]$  and  $(t_{\text{train}}, t_{\text{val}}]$ , respectively, where  $t_{\text{train}} = 1000$  and  $t_{\text{val}} = 1200$ . At each time point, the  $D \times D$  density matrix is represented as a vector with  $2D^2$  elements by stacking the real and imaginary parts. The plots with a green-yellow color map in Fig. S7 show the absolute error between the target and the predicted vector at  $M = 1$  and  $M = 5$ . The red points in these plots indicate the fidelities between the target and the predicted quantum states. We confirm that we can nearly reconstruct the previous depolarizing quantum channel almost perfectly as the fidelities are above 95% (with  $M = 5$ ).

Figure S8 illustrates an example of a simple moving average filter ( $\eta_i = 1$  for all  $i$ ) for a sequence of quantum channels  $\Omega_1, \Omega_2, \dots$  acting on the input states with the delay time  $d = 5, N_m = 5, N_e = 1$ , and the measurement multiplexity  $M = 1, 5$ . Other parameters are  $\alpha = 1.0, J/B = 1.0, t_{\text{buffer}} = 500, t_{\text{train}} = 1000$ , and  $t_{\text{val}} = 1200$ . Here, the input states jump to a new random quantum state every 20 time steps, thus introducing temporal dependencies between input states. Our framework can reconstruct this intriguing tomography of a simple moving average filter.

Figure S9 and Fig. S10 illustrate the other results for the tomography task  $F(\beta_n) = \Omega_{n-1}(\beta_{n-1})$  demonstrated in the main text. The first  $t_{\text{buffer}} = 1000$  time steps are excluded for initial transients to satisfy the QESP, the training and evaluating are performed in the range  $(t_{\text{buffer}}, t_{\text{train}}]$  and  $(t_{\text{train}}, t_{\text{val}}]$ , respectively, where  $t_{\text{train}} = 4000$  and  $t_{\text{val}} = 5000$ . Other model parameters are  $\alpha = 1.0, J/B = 1.0$ . Figure S9 illustrates the calculated RMSF as functions of  $N_m, N_e$ , and  $\tau B$  with the measurement multiplexity  $M = 1, 5$ , and the number of observables is  $K = N_m$ . The RMSF is averaged over ten different runs with random trials of the input sequence and initial state. We confirm that increasing  $N_m$  and  $M$  indeed scales the fidelity.

Figure S10 illustrates the calculated error (1.0 - RMSF) as functions of  $\tau B$  with the measurement multiplexity  $M = 5$  for different values of  $N_e, N_m$  and  $K$ . Here, the number of observables is set to  $K = N_m$  if we only select the observables as spin projections  $O_j = \hat{s}_j^z$  for all  $j$ , and to  $K = N_m(N_m + 1)/2$  if we further select the observables as two-spins correlations  $\hat{s}_i^z \hat{s}_j^z$  for all  $i < j$ . The error is averaged over ten different runs with random trials of the input sequence and initial state. The fidelity is larger than 94% even with  $N_e = 3$  qubits and  $N_m = 4, 5$ .

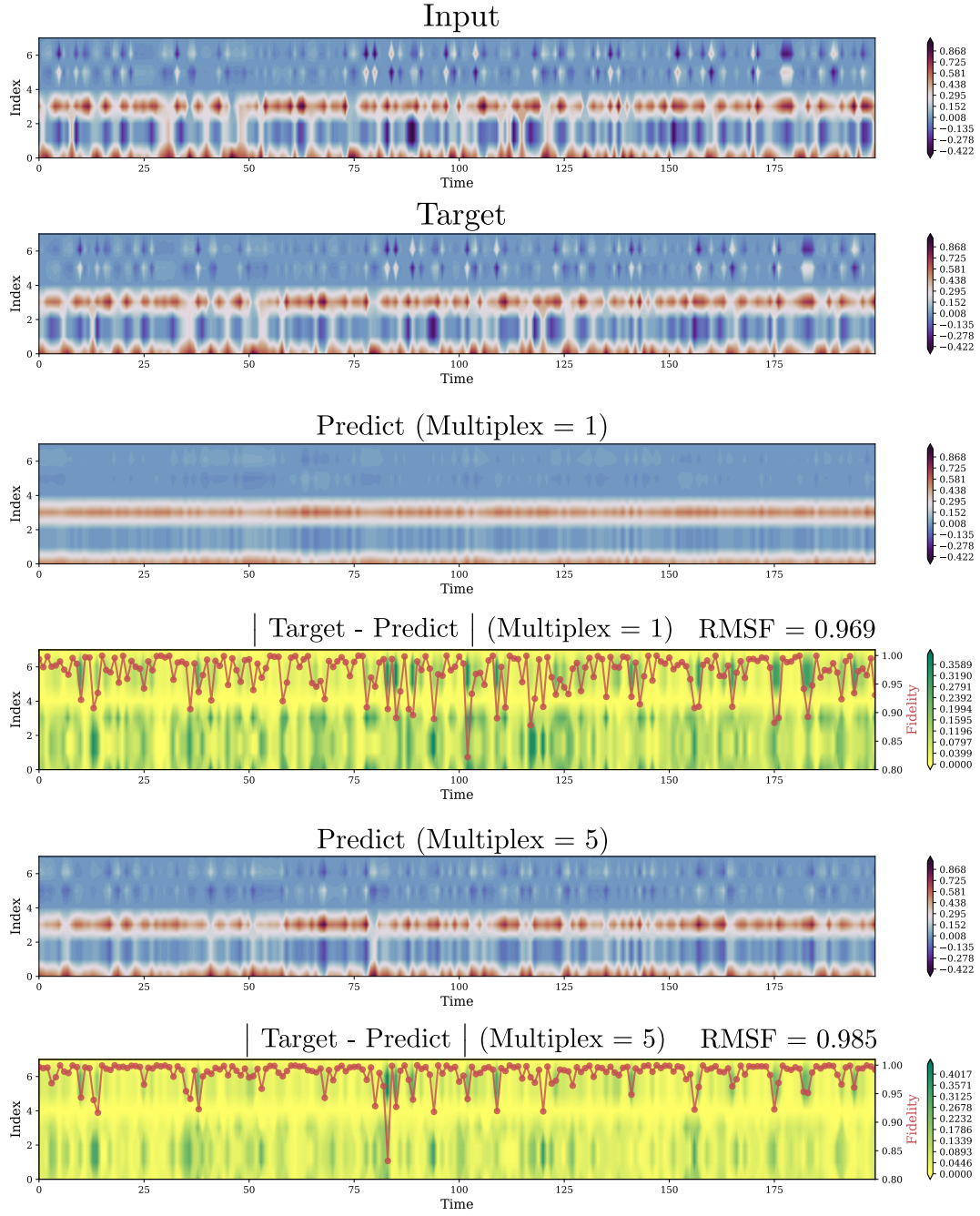


FIG. S7. Contour plots of a temporal forecast with the absolute difference between the target and the prediction for the reconstruction of depolarizing quantum channel with delay time  $d = 5$ ,  $N_m = 5$ , and  $N_e = 1$ . Other model parameters are  $\alpha = 1.0$ ,  $J = 1.0$ ,  $J/B = 1.0$ , and  $\tau B = 2.0$ . At each time point, the  $2 \times 2$  density matrix is represented as a vector with 8 elements by stacking the real and imaginary parts. The red points in the last plot (with right y-axis) represent the fidelities at each time point between the target and the predicted state.

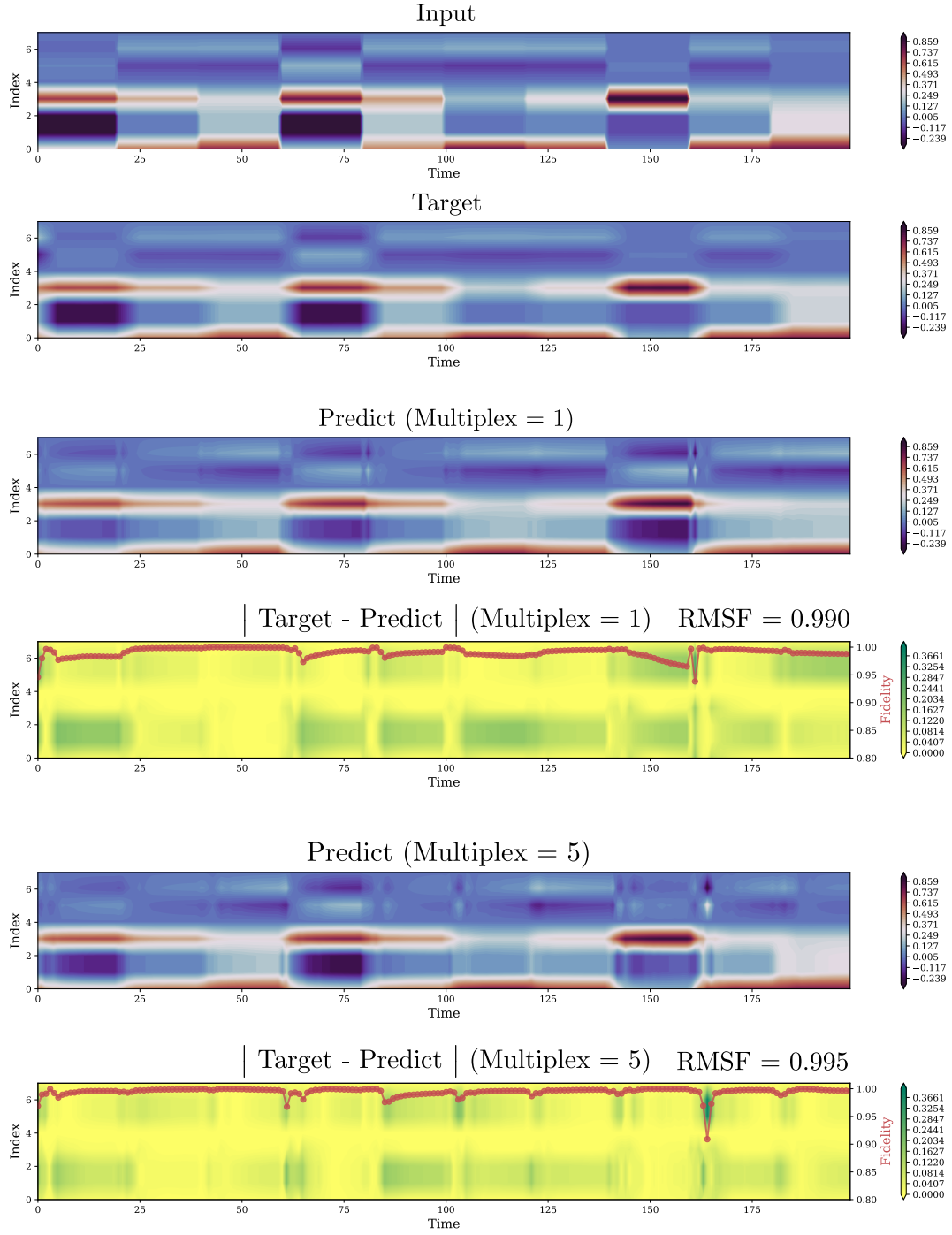


FIG. S8. Contour plots of a temporal forecast with the absolute difference between the target and the prediction for the reconstruction of a simple moving average filter for a sequence of depolarizing quantum channels with delay time  $d = 5$ ,  $N_m = 5$ , and  $N_e = 1$ . Other model parameters are  $\alpha = 1.0$ ,  $J = 1.0$ ,  $J/B = 1.0$ , and  $\tau B = 2.6$ . At each time point, the  $2 \times 2$  density matrix is represented as a vector with 8 elements by stacking the real and imaginary parts. The red points in the last plot (with right y-axis) represent the fidelities at each time point between the target and the predicted state.

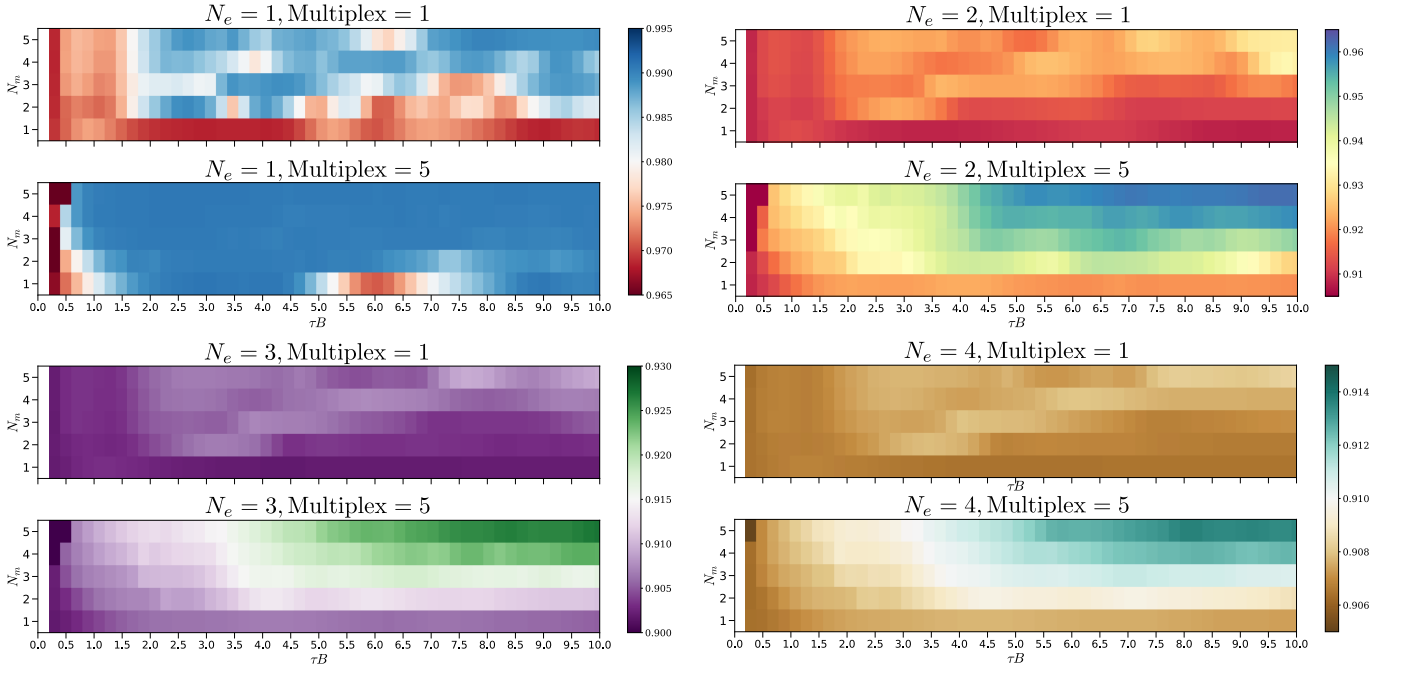


FIG. S9. Fidelities as functions of  $N_m, N_e$ , and the normalized interaction time  $\tau B$  for the memory-based reconstruction of depolarizing quantum channel with delay  $d = 1$ . The levels of fidelity values are indicated by the color bars.

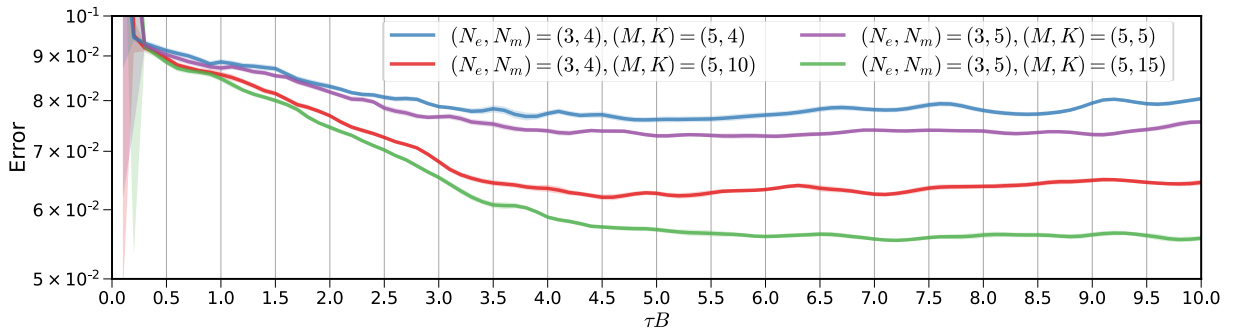


FIG. S10. Tomography errors for input states of  $N_e = 3$  qubits in fidelities as functions of  $\tau B$  for the reconstruction of depolarizing quantum channel  $\mathcal{F}(\beta_n) = \Omega_{n-d}(\beta_{n-d})$  with  $d = 1$ .

- 
- [1] H. Jaeger, [Bonn, Germany: German National Research Center for Information Technology GMD Technical Report 148, 13 \(2001\)](#).
  - [2] W. Maass, T. Natschlager, and H. Markram, [Neural Comput. 14, 2531 \(2002\)](#).
  - [3] M. Lukoševičius and H. Jaeger, [Comput. Sci. Rev. 3, 127 \(2009\)](#).
  - [4] G. Tanaka, T. Yamane, J. B. Heroux, R. Nakane, N. Kanazawa, S. Takeda, H. Numata, D. Nakano, and A. Hirose, [Neural Networks 115, 100 \(2019\)](#).
  - [5] K. Nakajima, [Jpn. J. Appl. Phys. 59, 060501 \(2020\)](#).
  - [6] K. Fujii and K. Nakajima, [Phys. Rev. Applied 8, 024030 \(2017\)](#).
  - [7] K. Nakajima, K. Fujii, M. Negoro, K. Mitarai, and M. Kitagawa, [Phys. Rev. Applied 11, 034021 \(2019\)](#).
  - [8] S. Ghosh, A. Opala, M. Matuszewski, T. Paterek, and T. C. Liew, [Npj Quantum Inf. 5, 1 \(2019\)](#).
  - [9] S. Ghosh, A. Opala, M. Matuszewski, T. Paterek, and T. C. H. Liew, [IEEE Trans. Neural Netw. Learn. Syst. , 1 \(2020\)](#).
  - [10] S. Ghosh, T. Paterek, and T. C. H. Liew, [Phys. Rev. Lett. 123, 260404 \(2019\)](#).
  - [11] J. Nokkala, R. Martınez-Pena, G. L. Giorgi, V. Parigi, M. C. Soriano, and R. Zambrini, [Preprint at arXiv:2006.04821 \(2020\)](#).
  - [12] L. C. G. Govia, G. J. Ribeill, G. E. Rowlands, H. K. Krovi, and T. A. Ohki, [Preprint at arXiv:2004.14965 \(2020\)](#).
  - [13] M. Negoro, K. Mitarai, K. Fujii, K. Nakajima, and M. Kitagawa, [Preprint at arXiv:1806.10910 \(2018\)](#).
  - [14] J. Chen, H. I. Nurdin, and N. Yamamoto, [Phys. Rev. Applied 14, 024065 \(2020\)](#).
  - [15] S. Dasgupta, K. E. Hamilton, and A. Banerjee, [Preprint at arXiv:2004.08240 \(2020\)](#).
  - [16] D. S. Abrams and S. Lloyd, [Phys. Rev. Lett. 83, 5162 \(1999\)](#).
  - [17] Y. Chen and X. Ye, [Preprint at arXiv:1101.6081 \(2011\)](#).
  - [18] B. I. Bantysh, A. Y. Chernyavskiy, and Y. I. Bogdanov, [Preprint at arXiv:2012.15656 \(2020\)](#).
  - [19] Q. H. Tran and K. Nakajima, [Preprint at arXiv:2006.08999 \(2020\)](#).
  - [20] J. Chen and H. I. Nurdin, [Quantum Inf. Process. 18 \(2019\), 10.1007/s11128-019-2311-9](#).
  - [21] M. A. Nielsen and I. L. Chuang, *Quantum Computation and Quantum Information: 10th Anniversary Edition*, 10th ed. (Cambridge University Press, USA, 2011).
  - [22] L. Bruneau, A. Joye, and M. Merkli, [Ann. Inst. H. Poincare Probab. Statist. 46, 442 \(2010\)](#).
  - [23] I. Nechita and C. Pellegrini, [Probab. Theory Relat. Fields 152, 299 \(2010\)](#).
  - [24] R. Movassagh and J. Schenker, [Preprint at arXiv:1909.11769 \(2019\)](#).
  - [25] R. Movassagh and J. Schenker, [“Theory of ergodic quantum processes,” \(2020\)](#).
  - [26] J. M. Steele, [Ann. Inst. H. Poincare Probab. Statist.s 25, 93 \(1989\)](#).
  - [27] H. Hennion, [Ann. Probab. 25, 1545 \(1997\)](#).
  - [28] D. Porras and J. I. Cirac, [Phys. Rev. Lett. 92, 207901 \(2004\)](#).
  - [29] K. Kim, M.-S. Chang, R. Islam, S. Korenblit, L.-M. Duan, and C. Monroe, [Phys. Rev. Lett. 103, 120502 \(2009\)](#).
  - [30] P. Jurcevic, B. P. Lanyon, P. Hauke, C. Hempel, P. Zoller, R. Blatt, and C. F. Roos, [Nature 511, 202 \(2014\)](#).
  - [31] K. Macieszczak, M. u. u. u. Gua, I. Lesanovsky, and J. P. Garrahan, [Phys. Rev. Lett. 116, 240404 \(2016\)](#).
  - [32] J. B. Lasserre, [IEEE Trans. Autom. Control. 40, 1500 \(1995\)](#).
  - [33] G. J. Szekely, M. L. Rizzo, and N. K. Bakirov, [Ann. Stat. 35, 2769 \(2007\)](#).
  - [34] H. Jaeger, [“Short term memory in echo state networks,” \(GMD-Forschungszentrum Informationstechnik, 2001\)](#).
  - [35] J. Dambre, D. Verstraeten, B. Schrauwen, and S. Massar, [Sci. Rep. 2 \(2012\), 10.1038/srep00514](#).
  - [36] A. Atiya and A. Parlos, [IEEE Trans. Neural Netw. Learn. Syst. 11, 697 \(2000\)](#).